NACA RM L53F23

NACA

RESEARCH MEMORANDUM

EFFECTS OF LEADING-EDGE SLATS ON THE AERODYNAMIC CHARACTERISTICS OF A 45° SWEEPBACK WING-FUSELAGE CONFIGURATION AT MACH NUMBERS OF 0.4 TO 1.03

By Jack F. Runckel and Seymour Steinberg

Langley Aeronautical Laboratory
Langley Field, Va.

Declassified January 24, 1958

NATIONAL ADVISORY COMMITTEE
FOR AERONAUTICS
WASHINGTON

August 21, 1953

NACA RM L53F23

NATIONAL ADVISORY COMMITTEE FOR AERONAUTICS

RESEARCH MEMORANDUM

EFFECTS OF LEADING-EDGE SLATS ON THE AERODYNAMIC CHARACTERISTICS OF A 45° SWEPTBACK WING-FUSELAGE CONFIGURATION AT MACH NUMBERS OF 0.4 TO 1.03

By Jack F. Runckel and Seymour Steinberg

SUMMARY

An investigation was conducted in the Langley 16-foot transonic tunnel to determine the aerodynamic characteristics of a wing-fuselage combination with a 45° sweptback wing having NACA 65A006 airfoil sections, an aspect ratio of 4, taper ratio of 0.6, and incorporating outboard leading-edge slats. Slats of 45 percent semispan and 0°, 10°, and 20° slat deflection, and 35 percent semispan having 0° and 10° deflection were tested at Mach numbers from 0.40 to 1.03. For each configuration all or parts of the Mach number range were investigated through an angle-of-attack range from -2° to 26° at the lowest speeds and from -2° to 8° at the highest speed at Reynolds numbers from 4×10^6 to 6.5×10^6.

The use of the slat configurations tested generally delayed the lift-curve break to higher angles of attack, increased the lift in the high angle-of-attack range, and reduced the drag and increased the lift-drag ratio at high lift coefficients for all Mach numbers. Although the slatted wing-fuselage configurations exhibited pitch-up, this tendency was less severe than for the basic wing-fuselage combination. All slat configurations produced a decrease in the nonlinearity of the pitching-moment curves and an extension of the lift coefficients for pitch-up. For the slat configurations investigated, it was found that the differences in spanwise extent and slat deflection had small and inconsistent effects on the model aerodynamic characteristics and that the aerodynamic gains obtained with slats generally decreased with increases in Mach number.

INTRODUCTION

Various wing-leading-edge high-lift devices have been used successfully to prevent unstable pitching-moment changes at or near the stall on many types of airplanes at low speeds. These devices have been used primarily as an aid during take-off and landing. Research on the low-speed aerodynamic characteristics of wings with various types of slats has, therefore, been quite extensive. Reference 1 presents a summary of the literature on the low-speed longitudinal characteristics of wings with extensible slats.

More recently, however, slats have been used as a high-speed implement as well as a low-speed device to improve the longitudinal stability characteristics of airplanes while in high-speed maneuvering flight. The available data at high speeds on the effect of slats on airplane and model aerodynamic characteristics are given in references 2 and 3. It has been shown not only that the unstable pitching-moment breaks experienced at high-lift coefficients and high Mach numbers have been delayed by the use of leading-edge slats, but also that the drag at these conditions has been substantially reduced (ref. 3), thus increasing the airplane maneuverability at high subsonic speeds.

As part of a general investigation of the effects of various wing-leading-edge devices upon the aerodynamic and longitudinal stability characteristics of a 45° sweptback wing-body model at transonic speeds, five outboard leading-edge slat configurations were tested in the Langley 16-foot transonic tunnel and the results are reported herein. Slats of two spanwise extents with two and three deflection angles were investigated. Results were obtained through a Mach number range from 0.40 or 0.60 (depending on the configuration) up to 1.03 at Reynolds numbers from 4×10^6 to 6.5×10^6 and at angles of attack from about -2° to 26° at the lowest test speeds and from -2° to 8° at the highest test speed.

SYMBOLS

C_L lift coefficient, L/qS

C_D drag coefficient, D/qS

C_m pitching-moment coefficient, $\frac{M_{\bar{c}/4}}{qS\bar{c}}$

L lift, lb

D	drag, lb
$M_{\bar{c}/4}$	pitching moment about quarter-chord point of mean aerodynamic chord, lb-ft
q	free-stream dynamic pressure, lb/sq ft
S	basic wing area, 9.0 sq ft
$b/2$	model semispan, 3.0 ft
$\bar{c}$	mean aerodynamic chord of basic wing, 1.531 ft
c	local chord, in.
z	thickness ordinate of airfoil section, in.
M	Mach number
R	Reynolds number of wing based on $\bar{c}$
P	pressure coefficient, $\frac{p_{local} - p}{q}$
P_{cr}	pressure coefficient for local sonic velocity
p	free-stream static pressure, lb/sq ft
α	angle of attack, deg
δ_s	slat deflection angle, deg (see fig. 1(b))
δ_e	angle of leading-edge chord-extension chord line relative to local wing chord line (positive value indicates droop)

Subscripts:

B	basic model
S	model with slats
max	maximum

MODEL AND APPARATUS

The investigation was conducted in the Langley 16-foot transonic tunnel, a full description of which is given in reference 4. As indicated in this reference, the maximum variation of the average Mach number along the test-section center line in the vicinity of the model is about ±0.002.

The wing-fuselage combination used in the present investigation was the same as that used for a general research program on a 45° sweptback wing-body arrangement at transonic speeds (see refs. 5 and 6). The steel wing had 65A006 airfoil sections parallel to the airstream, 45° sweep of the quarter-chord line, a taper ratio of 0.6, and an aspect ratio of 4. A general arrangement of the model with the wing without slats which corresponds to a slats-closed configuration, hereinafter known as the "basic wing," is shown in figure 1(a). The magnesium fuselage was a curved body of revolution having a fineness ratio of 12 that had been reduced in length by cutting off the rear portion to give a fineness ratio of 10. A complete description of the basic model and tunnel sting support system is given in reference 5.

For the present investigation, 14 percent of the chord at the leading edge of the wing from the 55-percent-semispan station outward was altered for installation of leading-edge slats. Details of the slat arrangements tested are presented in figure 1(b). The 14-percent-chord tapered slats were moved forward 9 percent of the chord along the chord line extended for the zero-slat-deflection configurations. The slat trailing-edge gap of 1.1 percent of the wing chord was held constant for all slats with the slat trailing edge forming the pivot point for the slat. The 0.45b/2 slats were tested at 0°, 10°, and 20° deflection. The 0.45b/2, $\delta_s = 10°$ slat arrangement and model with support system are shown in figure 2(a). The 0.35b/2 slats were deflected 0° and 10° only. The slats extended from the wing tip inboard, as low-speed information (ref. 1) indicated that this arrangement would probably provide the greatest improvement in the stability characteristics. The spanwise lengths of the slats, 35 and 45 percent of the semispan, were selected to conform with a leading-edge extension investigation (ref. 6).

The 0.35b/2 slats were supported by 6 brackets, and the 0.45b/2 slats by 7 brackets attached in a streamwise orientation to the wing. Wooden strips cemented to the flat undersurface of the brackets provided a smoother fairing for the air flow through the slat channels. A photograph of the underside of the 0.45b/2, $\delta_s = 10°$ slats is shown in figure 2(b).

An internal strain-gage balance was used to measure the forces and moments on the model. The discussion of the accuracy of the balance and other instrumentation given in reference 5 applies to the data of this paper. Wing-pressure-distribution measurements were obtained for part of the investigation by utilizing the existing orifices that remained on the left wing after the wing was altered for the installation of the slats. The chordwise and spanwise distribution of orifices, which is identical to that reported in reference 7 from the 15-percent-chord station rearward, is shown on figure 3.

TESTS AND CORRECTIONS TO THE DATA

Tests

The Reynolds number field of the present investigation is defined in figure 4. The tests were conducted over a Mach number range from 0.40 to 0.94 for the 0.35b/2 and 0.45b/2 slats deflected 10°. The 0.35b/2, $\delta_s = 0°$ configuration was tested at Mach numbers from 0.40 to 1.03 and the 0.45b/2, $\delta_s = 0°$ range includes speeds from a Mach number of 0.60 up to 1.03. The 0.45b/2 slats with 20° deflection were tested over a limited angle-of-attack range at Mach numbers from 0.60 to 1.00. Two ranges of angle of attack were obtained through the use of knuckle arrangements inserted in the sting between the model and support strut. The 10° knuckle installation shown in figure 2(a) allowed the model to be varied through an angle range from about 5° to 25°. A 0° knuckle resulting in a straight sting permitted testing from about -5° to 15°. For most slat configurations, both knuckles were used to obtain data through an angle-of-attack range up to the limit of the support-system strength. Balance force and moment data were obtained for all runs. Simultaneous force and pressure measurements were obtained where pressure distributions were desired.

Corrections to the Data

The angle-of-attack data have been corrected for model deflections caused by aerodynamic forces and moments but have not been corrected for stream angularity which is known to be negligible. Fuselage base pressures were found to be the same as for the model with the basic wing (presented in ref. 5). No adjustments for sting interference or model base pressures have been applied to the aerodynamic force and moment data or to the data of references 5 and 6 used in the comparisons in this paper.

The data of reference 8 indicate that the effect of boundary interference on models in the Langley 16-foot transonic tunnel is small and, therefore, no adjustments to the data for this effect have been attempted.

RESULTS AND DISCUSSION

The results of tests of leading-edge slat configurations on a 45° sweptback wing-body combination in the Langley 16-foot transonic tunnel are presented in the following figures:

	Figure
Force and moment characteristics with various slat configurations	5 and 6
Lift characteristics	7 and 8
Wing section pressure distributions	9 and 10
Drag characteristics	11, 12, and 13
L/D characteristics	14
Pitching-moment characteristics	15, 16, and 17

The results of the tests of the model with 0.45b/2 slats deflected 0° and 10° and the 0.35b/2 slats deflected 0° and 10° are presented in figure 5. The variations of angle of attack, drag coefficient and pitching-moment coefficient with lift coefficient are shown for each of the Mach numbers. Data for the basic wing, corresponding to a slats-closed configuration, are compared with the slat configurations on each of the figures. These data have been obtained from reference 5 for Mach numbers of 0.60 to 1.03. The data for the basic wing-fuselage combination at a Mach number of 0.40, however, have been obtained from reference 9. The limited data on the 0.45b/2, $\delta_s = 20°$ slats are presented in figure 6. These slats were tested only at some of the higher angles of attack where it was believed that differences in aerodynamic characteristics due to the greater slat deflection would be appreciable. The results at Mach number 0.60 are compared with the configuration having 0.45b/2 slats with 0° and 10° deflection and with the basic wing-fuselage data.

Lift Characteristics

The comparisons of the wing having various slat arrangements with the basic wing configuration (fig. 5) show that, in general, the use of slats results in extending the linear portion of the lift curves and in increasing the value of lift coefficient in the region above the lift-curve break. Only small shifts in the angle of attack for zero lift were indicated for the deflected slats.

The lift curves for 0.60 Mach number in figure 6 show that, with the 0.45b/2 slats extended ($\delta_s = 0^\circ$), and then deflected at 10° and 20°, the break in the lift curves occurred at successively higher angles of attack than that for the basic wing. The maximum value of lift obtained with a $\delta_s = 20^\circ$ slat was about the same as for the $\delta_s = 10^\circ$ slat at a Mach number of 0.60.

The variation of lift coefficient with Mach number for the four main slat configurations and the model with the basic wing is presented in figure 7. It would be expected from an examination of figure 5 that the maximum increases in lift for the slat configurations would occur at the highest angles of attack and that the differences at low angles would be small. The data of figure 7 at 5° angle of attack show the lifts to be about the same for all models as would be expected. At an angle of attack of 10° (near the lift-curve breaks at the higher speeds), the lifts obtained with slats having 0° deflection and with the basic wing were about the same, while the lift coefficients with the deflection slats were somewhat lower up to a Mach number of about 0.85. At higher speeds, all slats indicated higher lifts than the basic model. At higher angles of attack, the lift increase with slats over that for the basic wing was generally even larger (fig. 5).

The extension of the slats had little effect on values of lift-curve slope obtained up to a Mach number of 0.85 (fig. 8). Above this speed all wings with slats extended produced slightly higher lift-curve slopes than the basic wing.

Influence of Slats on Wing Pressure Distribution

The nature of the spanwise and chordwise loading distribution and flow field over a similar 45° basic sweptback wing has been studied by other investigators (refs. 7 and 10). These investigations have revealed that, for speeds up to a Mach number of about 0.80, the typical tip stall associated with sweptback wings at high angles of attack is primarily due to the spread of the leading-edge separation vortex. The progressive stall in the outboard regions is accompanied by an increase in loading over the inboard regions. At higher speeds, shock-induced separation becomes the primary cause of the reduction in loading over the outboard region of the wing. Shocks originating at the wing leading edge and at the wing trailing-edge body juncture and a shock due to the wing-fuselage combination may combine to produce large regions of separated flow near the wing tips.

Pressure-distribution measurements obtained concurrently with force data during the present investigation indicate the manner in which the loads on the basic wing have been altered by the presence of the slats. Pressure distributions for the inboard wing stations A and B (0.135b/2

and 0.25b/2) are not included in the figures since the pressure distribution for the wing with slats was generally found to be about the same as the basic wing at these stations for Mach numbers above 0.85. Some slight decreases in the loadings at station B for the wings with slats were found at Mach numbers below 0.85.

Typical section pressure distributions over the portion of the wing influenced by the slats are presented in figure 9 for the basic wing and for 0.45b/2 slats deflected 0°, 10°, and 20°. At low angles of attack the slats had no appreciable effect on the pressure distributions (see plots for $\alpha = 4^\circ$). With an increase in angle of attack to 8°, some loss in loading on the wings with slats at stations E and F (the central position of the slats) is apparent for Mach numbers up to about 0.90, but, since the total lift was about the same for the slotted and basic wings, the compensating load must be carried on the leading-edge portion of the wing and on the slat itself. The pressure distributions illustrated for 12° angle of attack (region where the basic wing began to stall at the higher speeds) represent conditions where the slats have produced increments in lift (see fig. 5). For this attitude, and at Mach numbers below 0.90, the loading over the inboard region of the wing is reduced while an increased loading is carried on the outboard portion of the wing with slats. The outboard sections of the basic wing show an indication of separated flow on the upper surface from the leading edge rearward. The main improvements for the slatted-wing configurations occur over these outboard wing sections where higher loads were obtained over the forward portion of the airfoil sections with slats having 0° and 10° deflection. The loadings obtained with the slats deflected 20° are similar to those for the basic wing and provide no reduction in separation in the tip region of the wing at higher speeds.

Chordwise pressure distributions for undeflected slats of 45 and 35 percent semispan extent are compared with pressure distributions over the basic wing in figure 10. In these plots, the pressure distributions at station D are directly influenced by the slat only for the 0.45b/2 slats, since the 0.35b/2 slats lie outboard of this station. Only relatively small differences in loading due to the change in spanwise extent occur except at a Mach number of 0.90 where the longer slats carry a higher loading over the central portion of the slats.

The pressure-distribution data have indicated that slats deflected moderate amounts tend to increase the loading in the tip region of the wing and to concentrate this loading over the forward section of the airfoil. The higher tip loadings are believed to result from the interruption of the spanwise flow toward the wing tip by the staggering action of the pressure distribution at the inboard edge of the slat and by the vortex originating at the side of the slat sweeping across the spanwise flow.

Drag Characteristics

Minimum drag coefficients for the configurations with extended slats were higher than those for the basic model (fig. 5) at all Mach numbers. Above a lift coefficient of about 0.45 all configurations with slats had less drag than the basic model. The lift coefficients at which the extended slat configurations caused decreases in drag (that is, the "cross-over" lift coefficients) varied from about 0.10 to 0.45 depending on the configuration and speed. This "cross-over" lift coefficient becomes important if self-opening slats, actuated by the pressure distribution over the slat, are to be used in maneuvering flight at high speeds. Aerodynamic data such as that presented in figure 5 can be used to indicate the angles of attack at which the slat should be extended to obtain decreases in drag.

Figure 11 shows that the drag-rise Mach number for low and moderate lift coefficients is not affected by extension of the slats. The extension of the slats does, however, have a pronounced effect on the magnitude of the drag coefficient, the magnitude of the effect depending on the Mach number and lift coefficient. For the zero lift condition the deflected slats give a minimum drag almost double that of the basic wing; the undeflected slats had a somewhat smaller detrimental effect. At a lift coefficient of 0.8 the reduction in drag through the use of slats amounted to as much as 30 percent in the region of Mach numbers 0.90 to 0.95. These large reductions in drag obtained with slats at high lift coefficients could result in greater speeds or better maneuvering characteristics in tactical maneuvers provided serious instability problems which are apt to occur in this lift coefficient and Mach number range are avoided. The curves of figure 11 show that the $0.45b/2$ slats were more effective than the $0.35b/2$ slats in producing a reduction in drag at high lift coefficients. Past research (ref. 11) has demonstrated that an even greater reduction in drag may be possible by further increases in the spanwise extent of slats.

The effectiveness of slats in reducing drag at high lift coefficients and low speeds is thought to be accomplished by a reduction in separation. At high speeds, it is believed that a similar action occurs. Comparisons of the drag characteristics of the wing-body combination having slats with the same wing-body having leading-edge chord-extensions (ref. 6) have shown that the wing with slats had lower drags in the high lift coefficient and high subsonic Mach number range. If adjustments are made for the difference in the total wing area with slats and with chord extensions, the adjustments will account for only about one-third of the difference in drag between the configurations in this range of operation. This lower drag indicates that a slotted passage may provide an additional means of controlling separation on sweptback wings at high subsonic speeds. Typical pressure distributions for the wing with 15-percent-chord undeflected slats and with 15-percent-chord leading-edge

extensions with zero deflection (which simulate a slat without a slot passage) are illustrated in figure 12. The lower pressure coefficients, apparent directly behind the slats, are evidence of higher local velocities in this region due to the slot flow. An indication of the relative pressure-drag coefficients obtained with the basic wing and the wing with slats and the wing with chord-extensions can be seen from figure 13. For the portion of the chord for which data are available, both the slats and chord-extensions indicate lower pressure drag than that for the basic wing. Since the pressure distributions on the lower surface are about the same for all configurations to 15 percent chord ($z/c = 0.0219$), the larger area under the curve on the upper surface (thrust) for the slats will result in less net section drag for this configuration. The pressure distributions over the slat and chord-extension are unknown at this speed, but the preceding remarks would still be valid if the load over the slats were assumed uniform and equal to the values on the wing at the 15-percent-chord station. Loads data for deflected slats (refs. 3 and 12) and unpublished data for undeflected slats indicate negative chord-force (thrust) values for the slats themselves at the higher angles of attack which indicate that the above assumption is valid.

Lift-Drag Ratio Characteristics

The lift and drag characteristics of the slat configurations previously considered may be expected to show correlative effects on the lift-drag ratios. If extensible slats are to be used to improve landing and take-off characteristics and as an aid in high-speed maneuvers such as tight turns, high values of L/D at high lift coefficients are required. Figure 14 presents the variation of the ratio of L/D for slats to the L/D of the basic model with lift coefficient at several Mach numbers, which illustrates the gains that might be expected through the use of slats. The lift coefficients for maximum L/D of the basic model are indicated by ticks in the figure. At practically all speeds, the slats start to show an improvement in the airplane efficiency at lift coefficients of about 0.4. The undeflected slats appear to have a less detrimental effect than deflected slats at lift coefficients below 0.4. The greatest improvement in lift-drag ratio at high lift coefficients took place at Mach number 0.90 for all slat configurations. The slats which produced the greatest improvement in L/D at higher lift coefficients over the test speed range were the $0.45b/2$, $\delta_s = 10^\circ$ devices. The benefits of the use of slatted wings for increasing L/D generally decreased at Mach numbers above 0.94.

Pitching-Moment Characteristics

An examination of the pitching-moment curves of figure 5 reveals that the use of slats made the pitching-moment curves more nearly linear

and extended the pitch-up to higher values of lift coefficients at the higher speeds. It was found that the pitch-up in practically all cases was much less severe for the slat configurations than with the basic wing for this model without a horizontal tail. The improvement in stability characteristics obtained with slats is in agreement with high-speed data on wings with this type of high-lift device (ref. 3). The model with 0.35b/2 slats generally had slightly better stability characteristics than those with 0.45b/2 slats in the speed range below a Mach number of 0.98. These results are consistent with those for 15-percent-chord outboard leading-edge chord-extensions (ref. 6) where the effect of spanwise extent on the stability was also relatively small. Deflecting the slats for both the 0.35b/2 and 0.45b/2 extent generally resulted in a more stable wing-body combination in the high-lift-coefficient range up to Mach number 0.90. Even though the slats did not eliminate the pitch-up, they did extend the point at which severe stability changes occur to high values of lift coefficient. This is illustrated in figure 15 which indicates extensions in lift coefficient for the stability breaks from 0.3 to 0.4 at the lowest speeds and of 0.1 at a Mach number of 0.98 for the model with slats. The solid points indicate that maximum lift was not reached or that no severe stability changes were obtained up to the highest lift coefficient of the test.

The pitching-moment-coefficient variation with Mach number was similar for all slat configurations at a lift coefficient of 0.4 (fig. 16(a)). At a lift coefficient of 0.8 (fig. 16(b)), all slat configurations have a greater nose-down tendency than the basic wing since at this lift coefficient the basic wing was well into the pitch-up range. Comparisons of the static-stability-parameter curves of figure 17 show that the addition of leading-edge slats to the basic wing had a negligible effect at zero lift, but at a lift coefficient of 0.4 all extended slats caused a forward shift in the aerodynamic-center position of approximately 5 percent of the chord; this shift decreased slightly at the higher speeds. Although the longitudinal stability characteristics for these slats of two spanwise extents and with three deflection angles were all somewhat similar, the results indicate that a slat configuration of about 40 percent semispan and with a deflection of less than 10° may provide more consistent stability improvements than the slats tested.

CONCLUDING REMARKS

The aerodynamic characteristics of a 45° sweptback wing-fuselage combination with outboard leading-edge slats of 45 percent semispan and 0°, 10°, and 20° slat deflection, and 35-percent-semispan slats having 0° and 10° deflection were investigated at Mach numbers of 0.4 to 1.03.

The addition of these slat configurations to the basic wing model resulted in extending the onset of stall to higher angles of attack, increasing zero-lift drag, decreasing the lift-drag ratio at low lift coefficients, and increasing the lift-drag ratio at high lift coefficients for all Mach numbers. The incorporation of the slat configurations on the wing usually resulted in increasing the linearity of the pitching-moment curves and in extending the lift coefficient for pitch-up to higher values. In general, the 45-percent-semispan slat configurations had somewhat better lift-drag-ratio characteristics than the 35-percent-semispan slats, while the 35-percent-semispan slats had slightly better stability characteristics over most of the speed range. No consistent effects of moderate slat deflection angle on the model aerodynamic characteristics existed in the Mach number range investigated. However, the results indicate that a more optimum slat configuration for the wing used in the present investigation would represent a compromise between the two slat extents tested and a moderate slat deflection of less than 10°.

Langley Aeronautical Laboratory,
National Advisory Committee for Aeronautics,
Langley Field, Va., June 12, 1953.

REFERENCES

1. Furlong, G. Chester, and McHugh, James G.: A Summary and Analysis of the Low-Speed Longitudinal Characteristics of Swept Wings at High Reynolds Number. NACA RM L52D16, 1952.

2. Sjoberg, S. A., and Champine, R. A.: Preliminary Flight Measurements of the Static Longitudinal Stability and Stalling Characteristics of the Douglas D-558-II Research Airplane (BuAero No. 3794). NACA RM L9H31a, 1949.

3. Kelly, John A., and Hayter, Nora-Lee F.: Aerodynamic Characteristics of a Leading-Edge Slat on a 35° Swept-Back Wing for Mach Numbers From 0.30 to 0.88. NACA RM A51H23, 1951.

4. Ward, Vernon G., Whitcomb, Charles F., and Pearson, Merwin D.: Air-Flow and Power Characteristics of the Langley 16-Foot Transonic Tunnel With Slotted Test Section. NACA RM L52E01, 1952.

5. Hallissy, Joseph M., and Bowman, Donald R.: Transonic Characteristics of a 45° Sweptback Wing-Fuselage Combination - Effect of Longitudinal Wing Position and Division of Wing and Fuselage Forces and Moments. NACA RM L52K04, 1953.

6. West, F. E., Jr., Liner, George, and Martz, Gladys S.: Effect of Leading-Edge Chord-Extensions on the Aerodynamic Characteristics of a 45° Sweptback Wing-Fuselage Combination at Mach Numbers of 0.40 to 1.03. NACA RM L53B02, 1953.

7. Solomon, William, and Schmeer, James W.: Effect of Longitudinal Wing Position on the Pressure Characteristics at Transonic Speeds of a 45° Sweptback Wing-Fuselage Model. NACA RM L52K05a, 1953.

8. Whitcomb, Charles F., and Osborne, Robert S.: An Experimental Investigation of Boundary Interference on Force and Moment Characteristics of Lifting Models in the Langley 16- and 8-Foot Transonic Tunnels. NACA RM L52L29, 1953.

9. Sutton, Fred B., and Martin, Andrew: Aerodynamic Characteristics Including Pressure Distributions of a Fuselage and Three Combinations of the Fuselage With Sweptback Wings at High Subsonic Speeds. NACA RM A50J26a, 1951.

10. Whitcomb, Richard T., and Kelly, Thomas C.: A Study of the Flow Over a 45° Sweptback Wing-Fuselage Combination at Transonic Mach Numbers. NACA RM L52D01, 1952.

11. Graham, Robert R., and Conner, D. William: Investigation of High-Lift and Stall-Control Devices on an NACA 64-Series 42° Sweptback Wing With and Without Fuselage. NACA RM L7G09, 1947.

12. Cahill, Jones F., and Nuber, Robert J.: Aerodynamic Load Measurements Over a Leading-Edge Slat on a 40° Sweptback Wing at Mach Numbers From 0.10 to 0.91. NACA RM L52G18a, 1952.

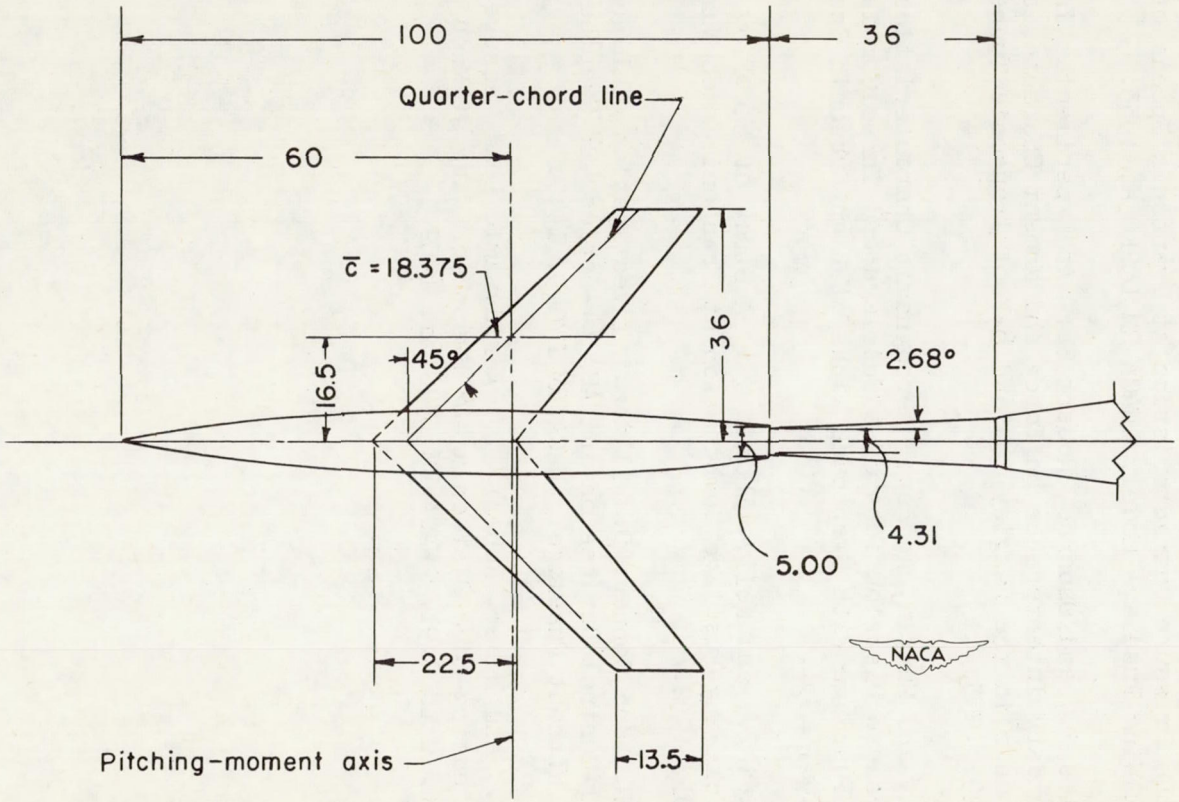

(a) Model with basic wing.

Figure 1.- Model plan form and slat details. All dimensions in inches.

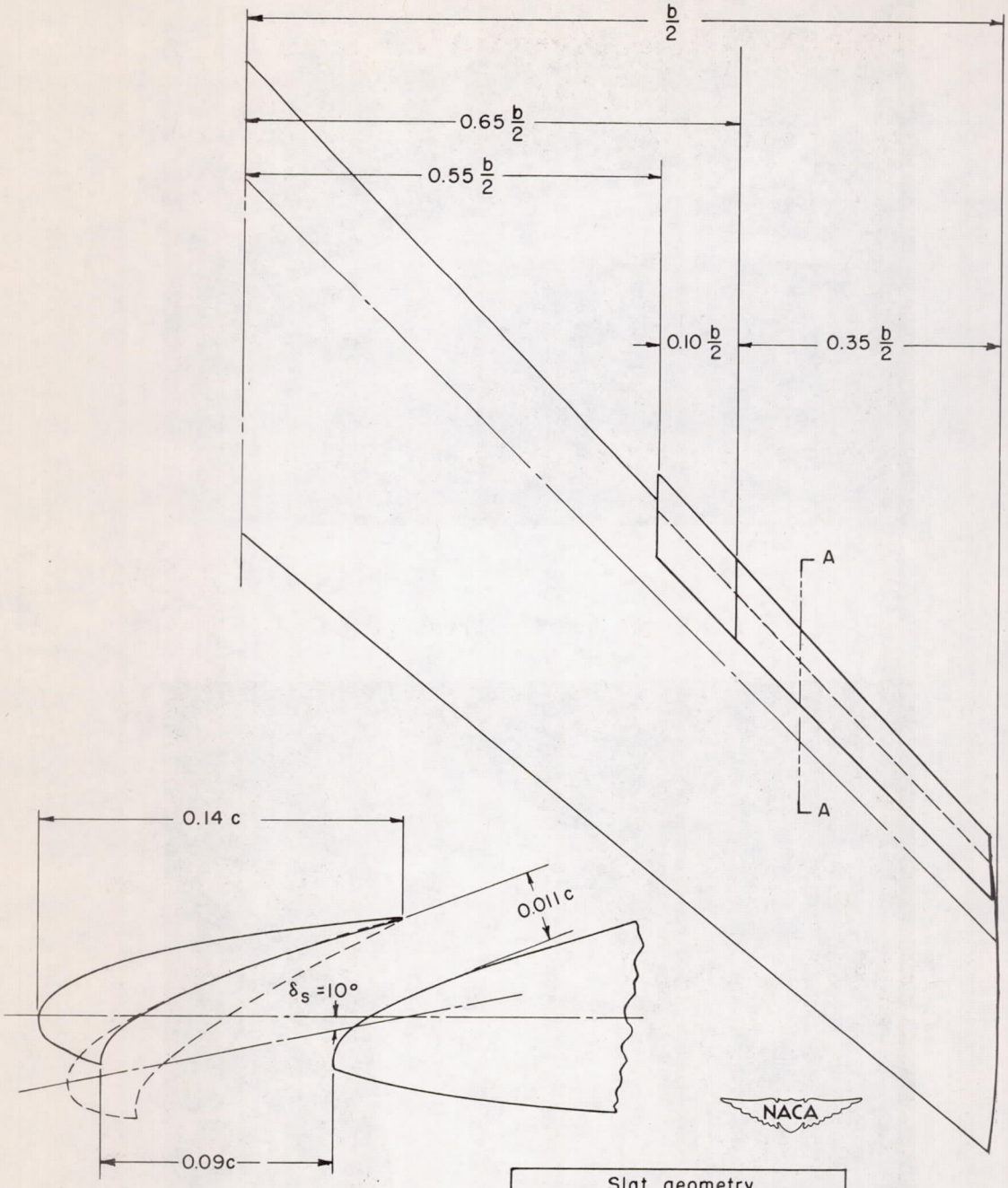

Section A-A

Slat geometry		
Deflection δ°	Extension % chord	Gap % chord
0	9.0	1.1
10	8.3	1.1
20	7.2	1.1

(b) Slat details.

Figure 1.- Concluded.

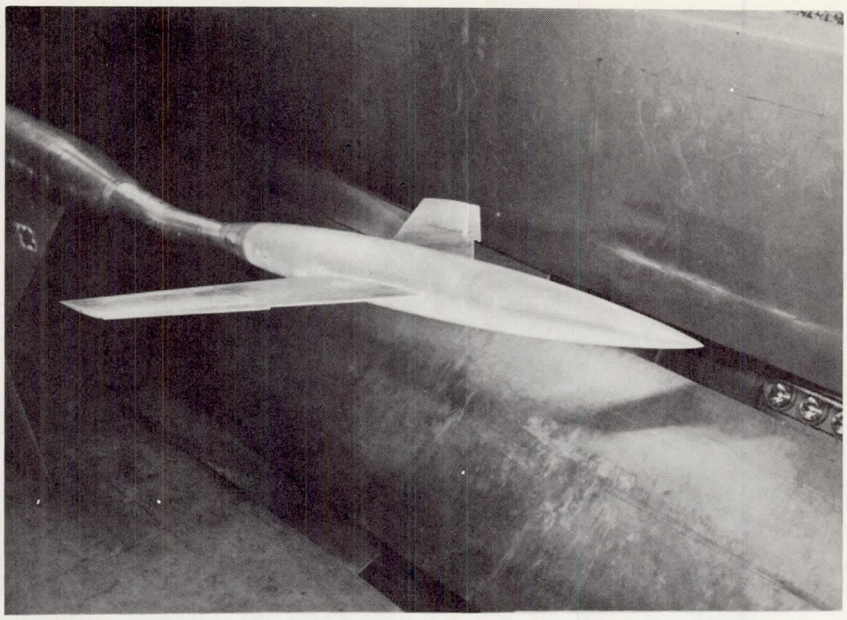

L-73545

(a) Three-quarter front view.

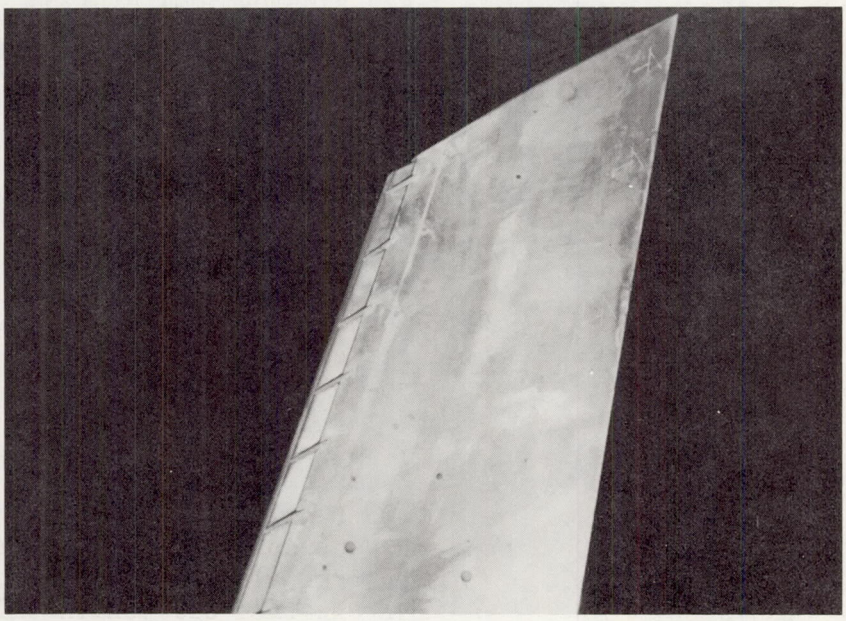

L-73544

(b) Underside showing slat support members.

Figure 2.- Wing-fuselage combination with 0.45b/2, $\delta_s = 10^\circ$ slats mounted on model support system.

Wing orifice station
location in percent of semispan

A	13.5
B	25.0
C	40.0
D	55.0
E	70.0
F	85.0
G	95.0

Wing orifice locations for stations A, B & C

Percent chord	
0	45.00
1.25	50.00
2.50	55.00
5.00	60.00
7.50	65.00
10.00	70.00
15.00	75.00
20.00	80.00
25.00	85.00
30.00	90.00
35.00	95.00
40.00	

Wing orifice locations for stations D, E, F, & G

Percent chord	
15.00	60.00
20.00	65.00
25.00	70.00
30.00	75.00
35.00	80.00
40.00	85.00
45.00	90.00
50.00	95.00
55.00	

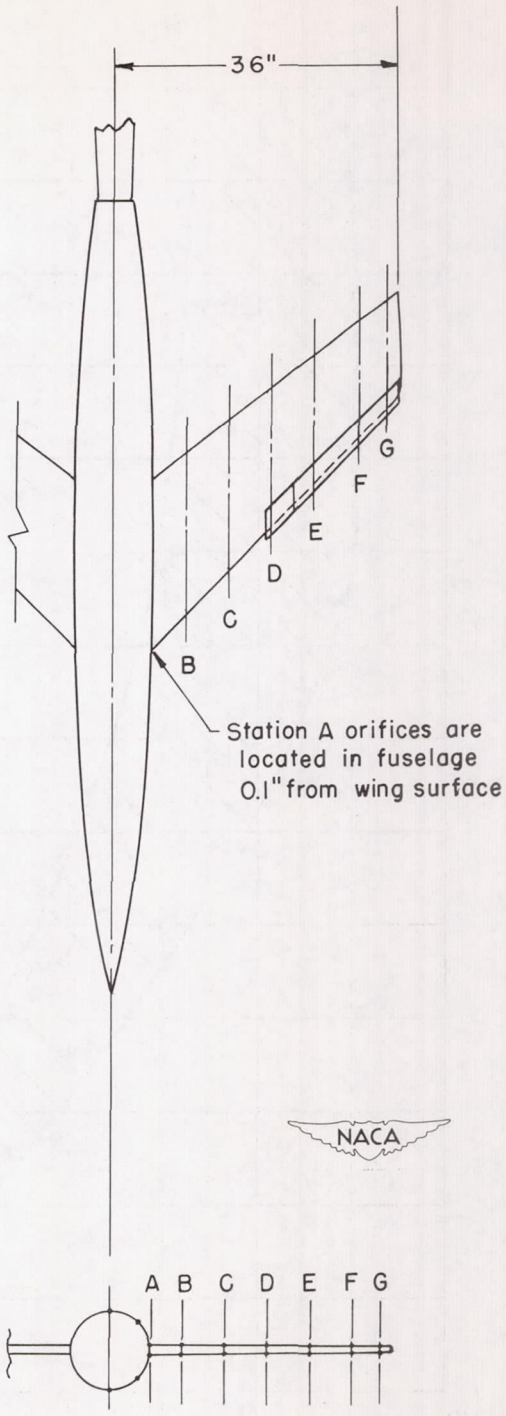

Figure 3.- Location of pressure orifices on wing-fuselage combination with slats.

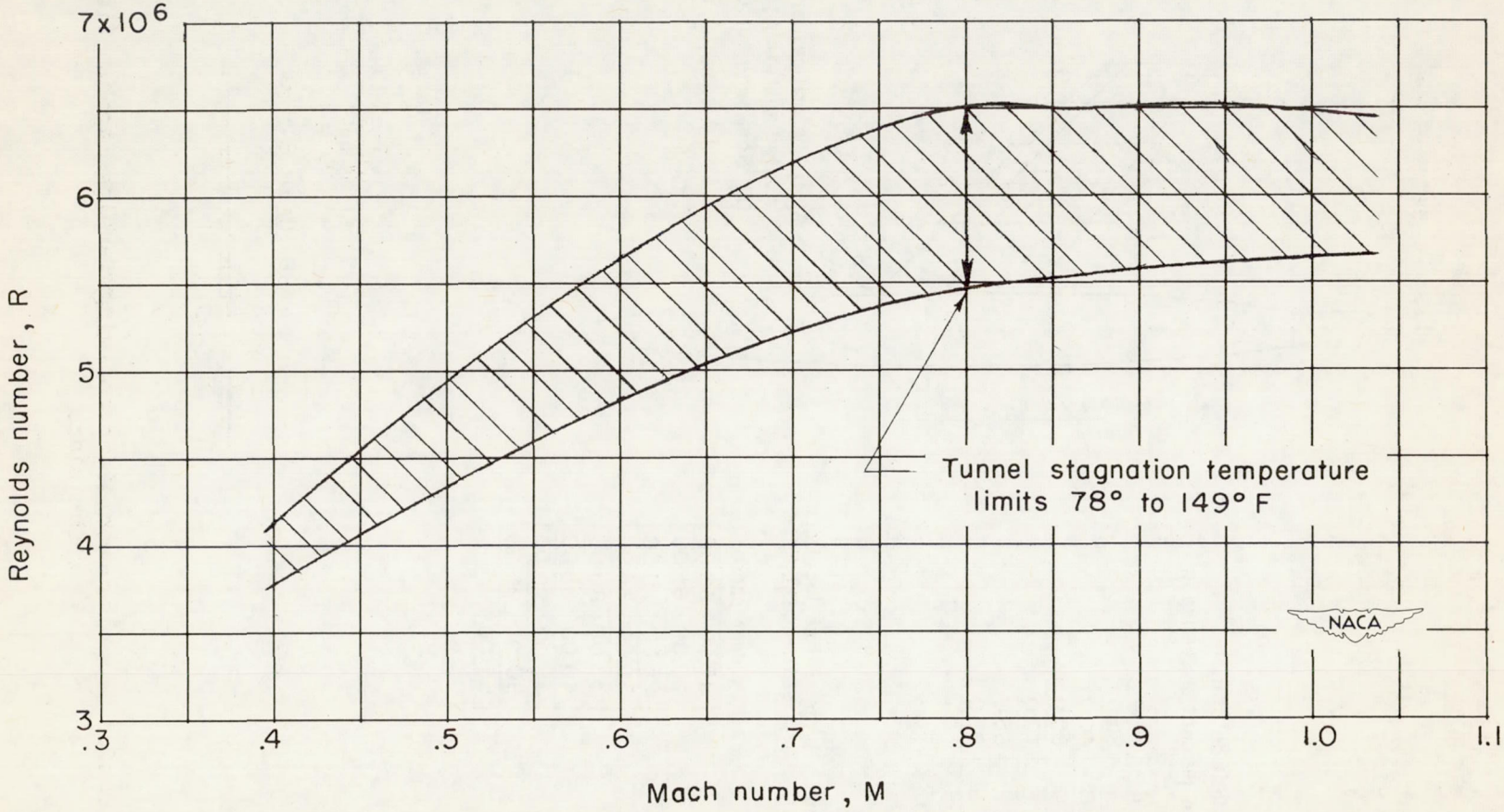

Figure 4.- Variation of Reynolds number with Mach number obtained in the investigation of the wing-fuselage combination with slats in the Langley 16-foot transonic tunnel. Reynolds number based on $\bar{c}$ = 1.531 feet.

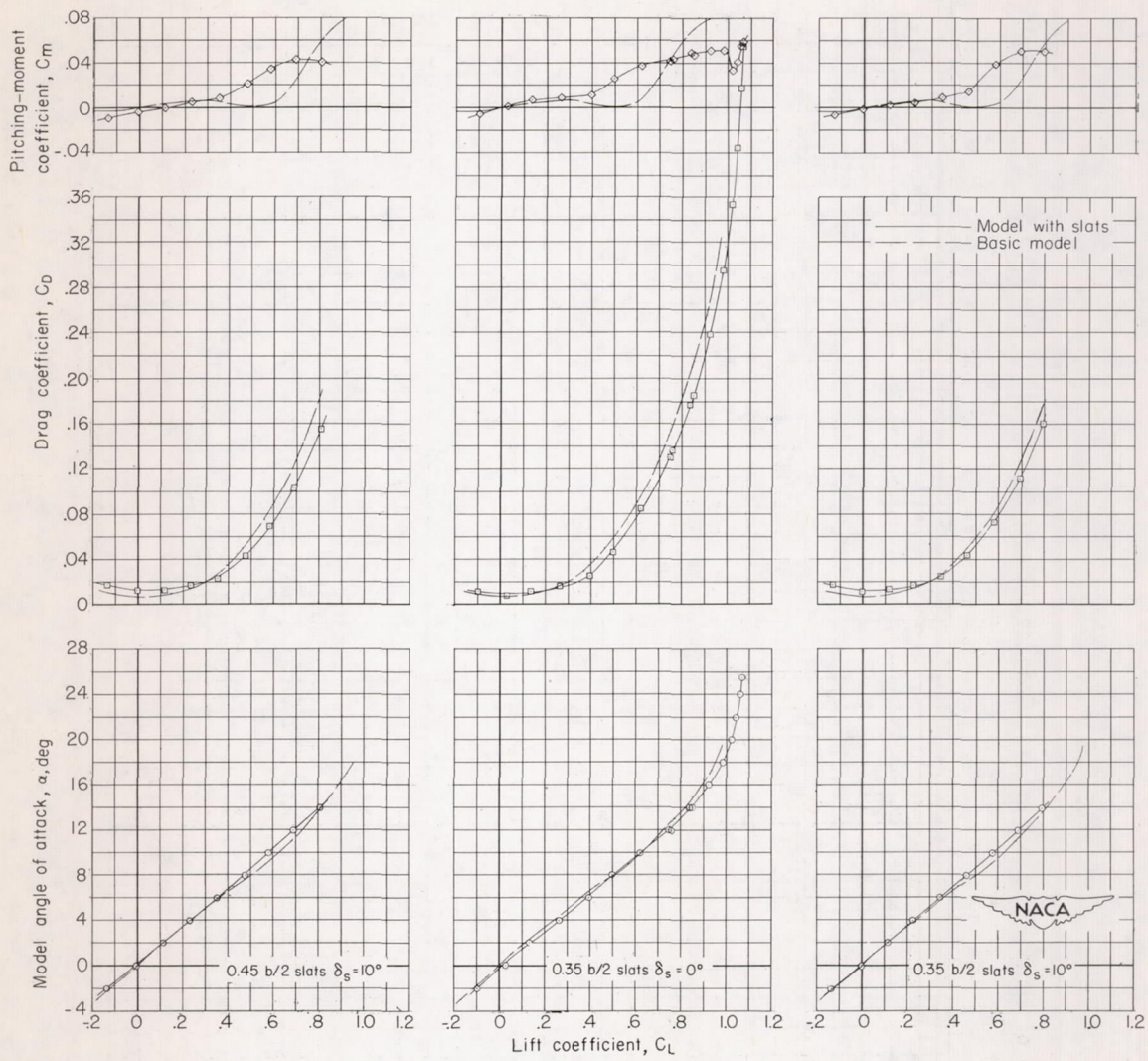

(a) M = 0.40. 0.45b/2 slats, $\delta_s = 10^\circ$; 0.35b/2 slats, $\delta_s = 0^\circ$ and 10°. Data for basic model from reference 9.

Figure 5.- Aerodynamic characteristics obtained from tests of wing-fuselage combination with various slat configurations.

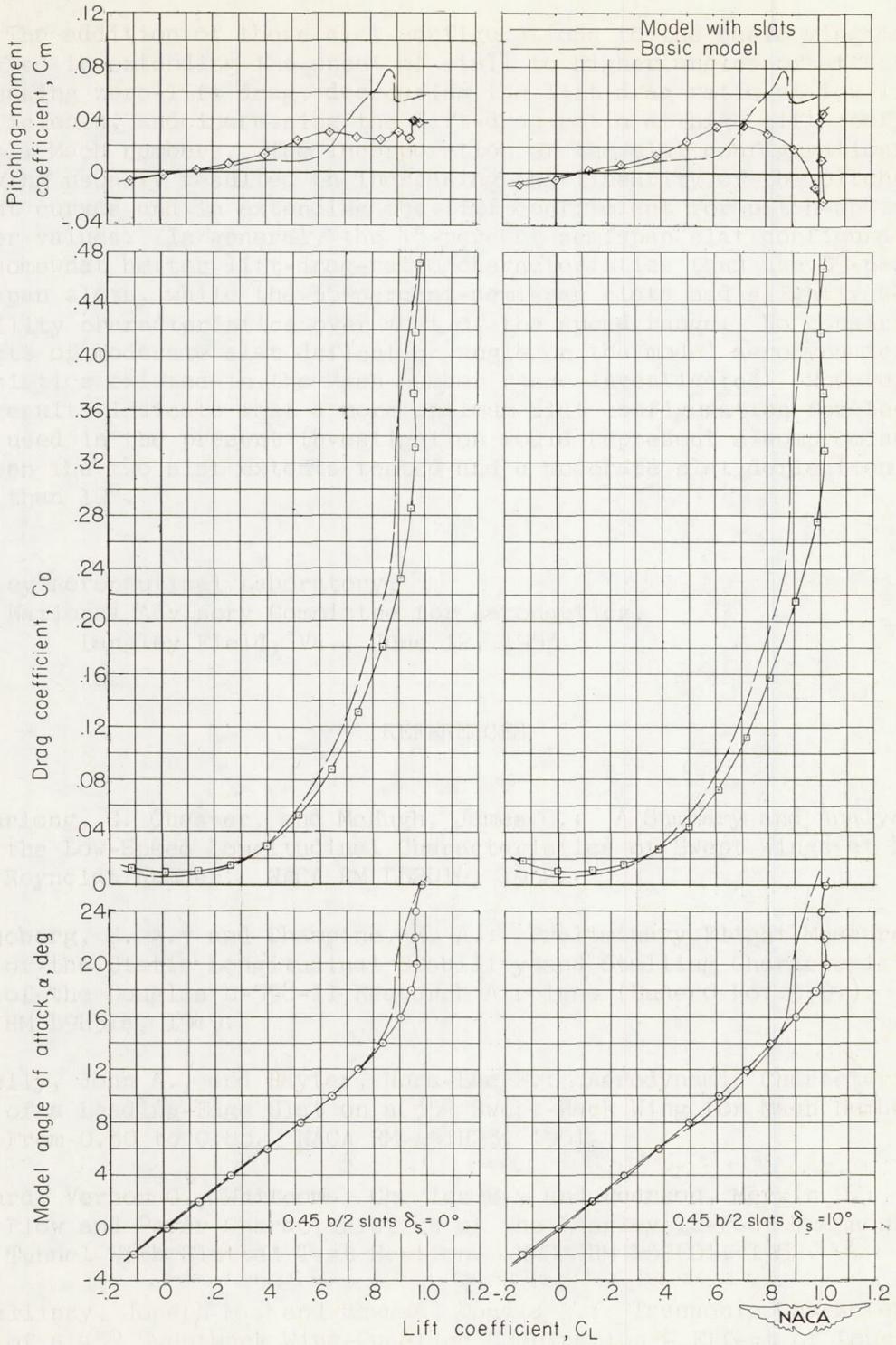

(b) M = 0.60. 0.45b/2 slats, δ_s = 0° and 10°.

Figure 5.- Continued.

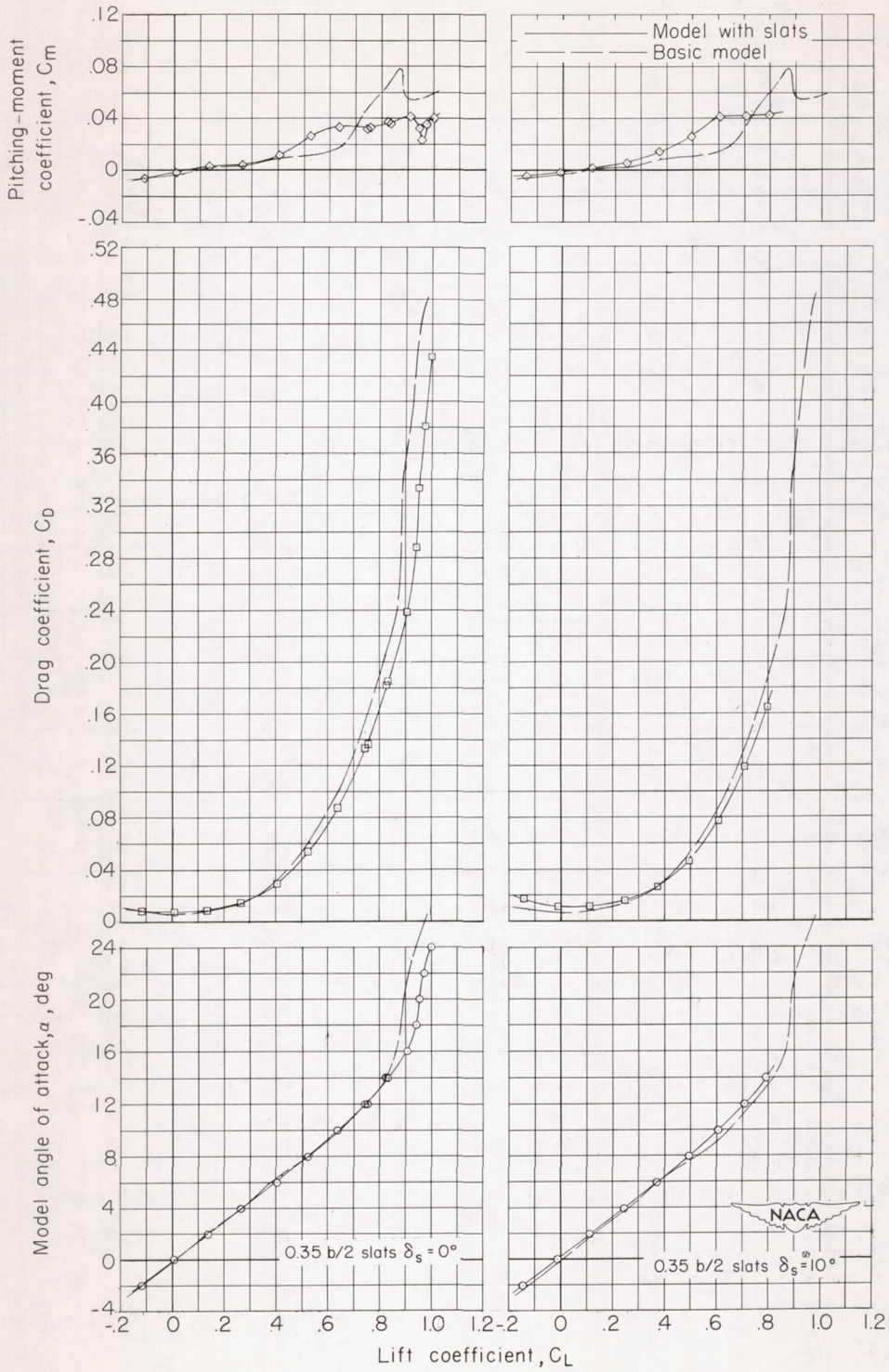

(c) M = 0.60. 0.35b/2 slats, $\delta_s = 0^\circ$ and 10°.

Figure 5.- Continued.

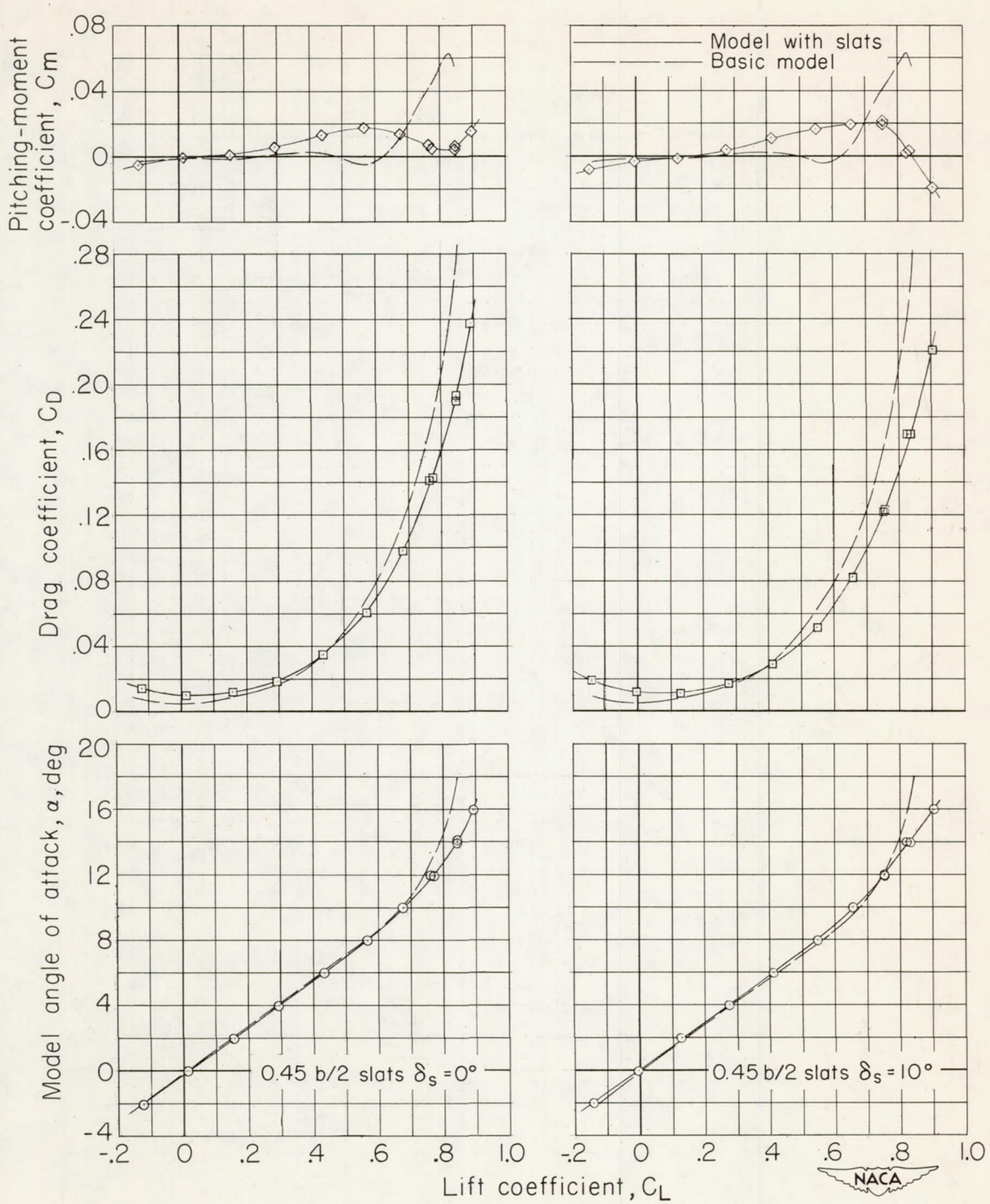

(d) M = 0.80. 0.45b/2 slats, δ_s = 0° and 10°.

Figure 5.- Continued.

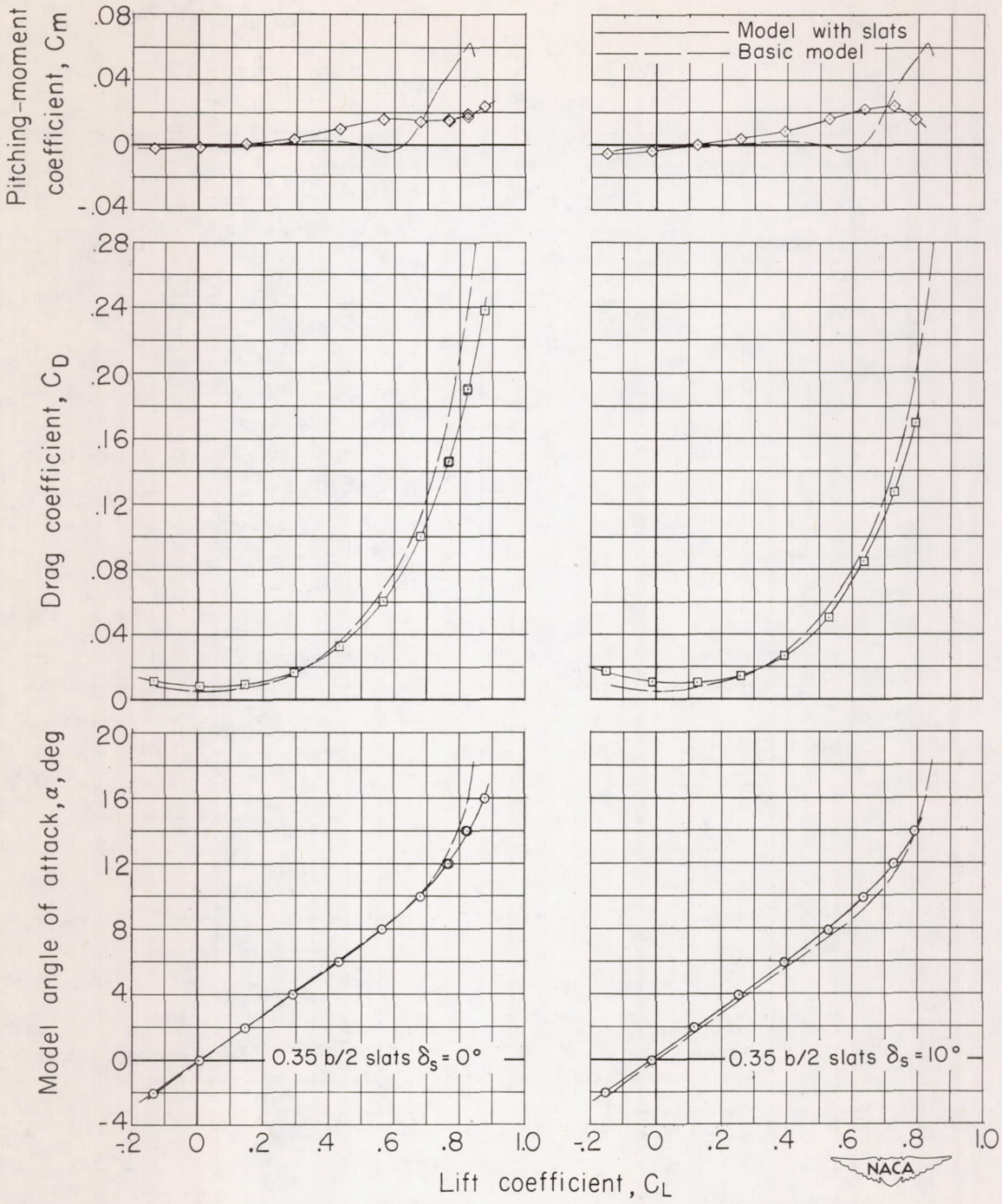

(e) M = 0.80. 0.35b/2 slats, $\delta_s = 0°$ and $10°$.

Figure 5.- Continued.

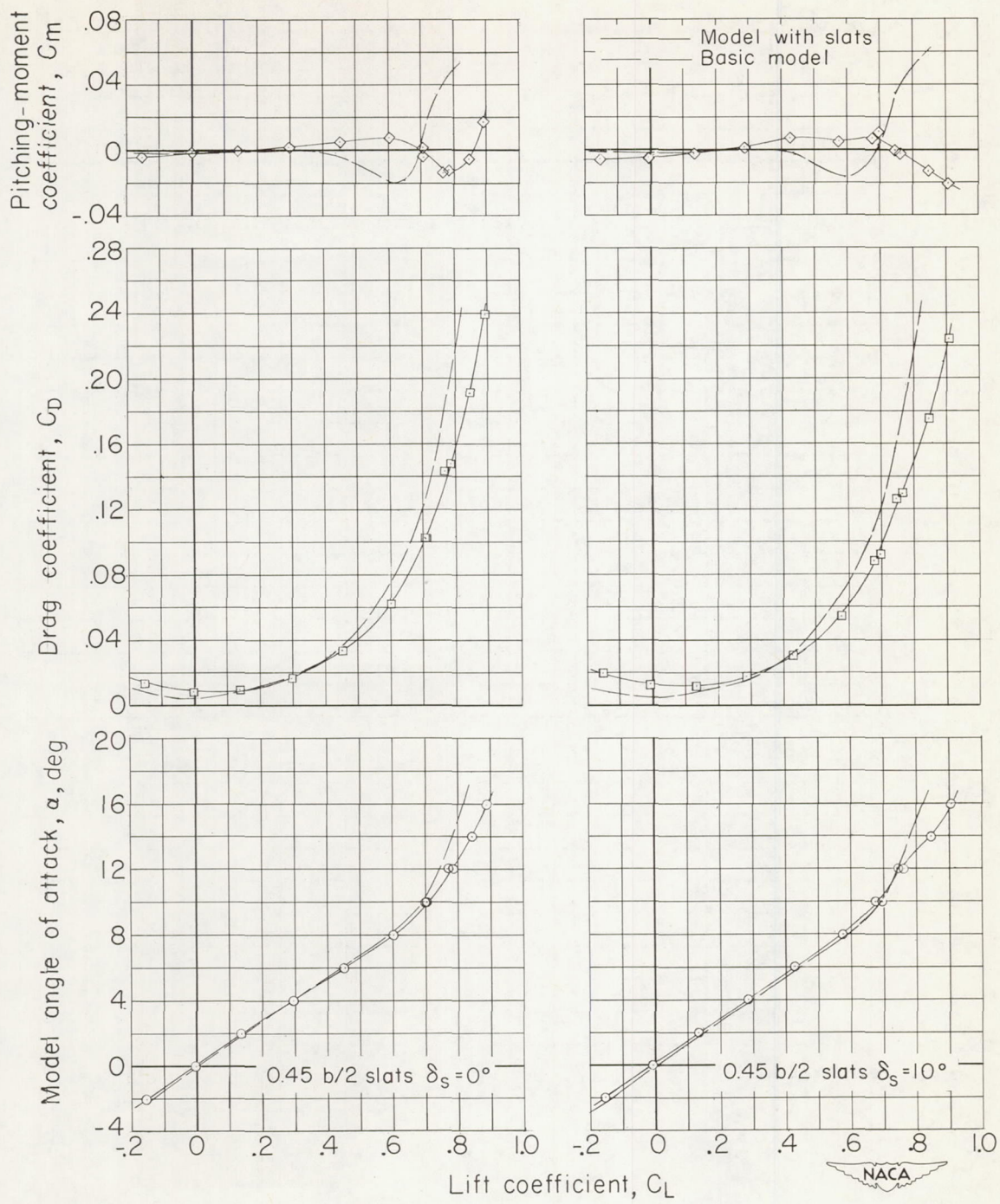

(f) M = 0.85. 0.45b/2 slats, δ_s = 0° and 10°.

Figure 5.- Continued.

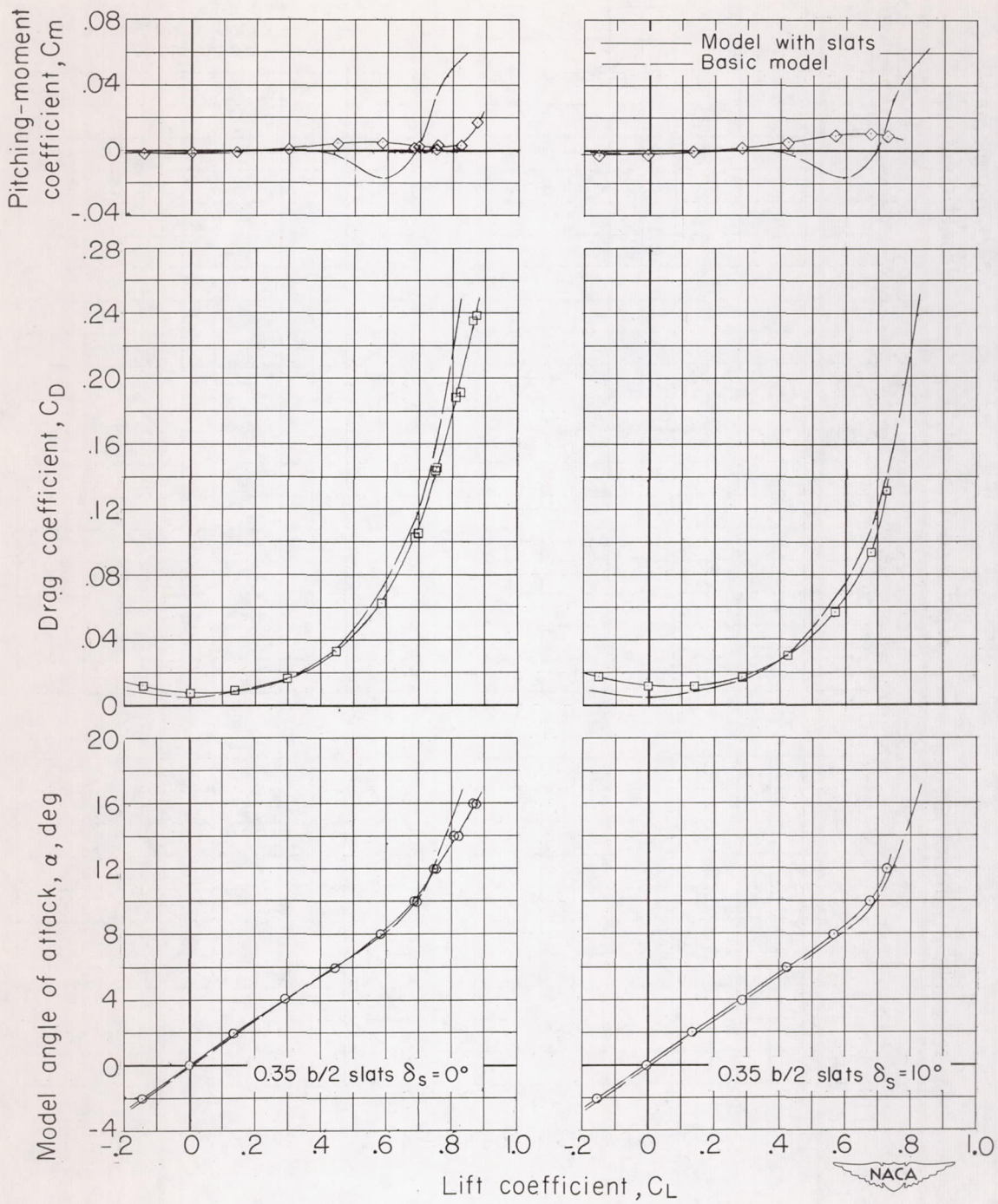

(g) M = 0.85. 0.35b/2 slats, $\delta_s = 0^\circ$ and 10°.

Figure 5.- Continued.

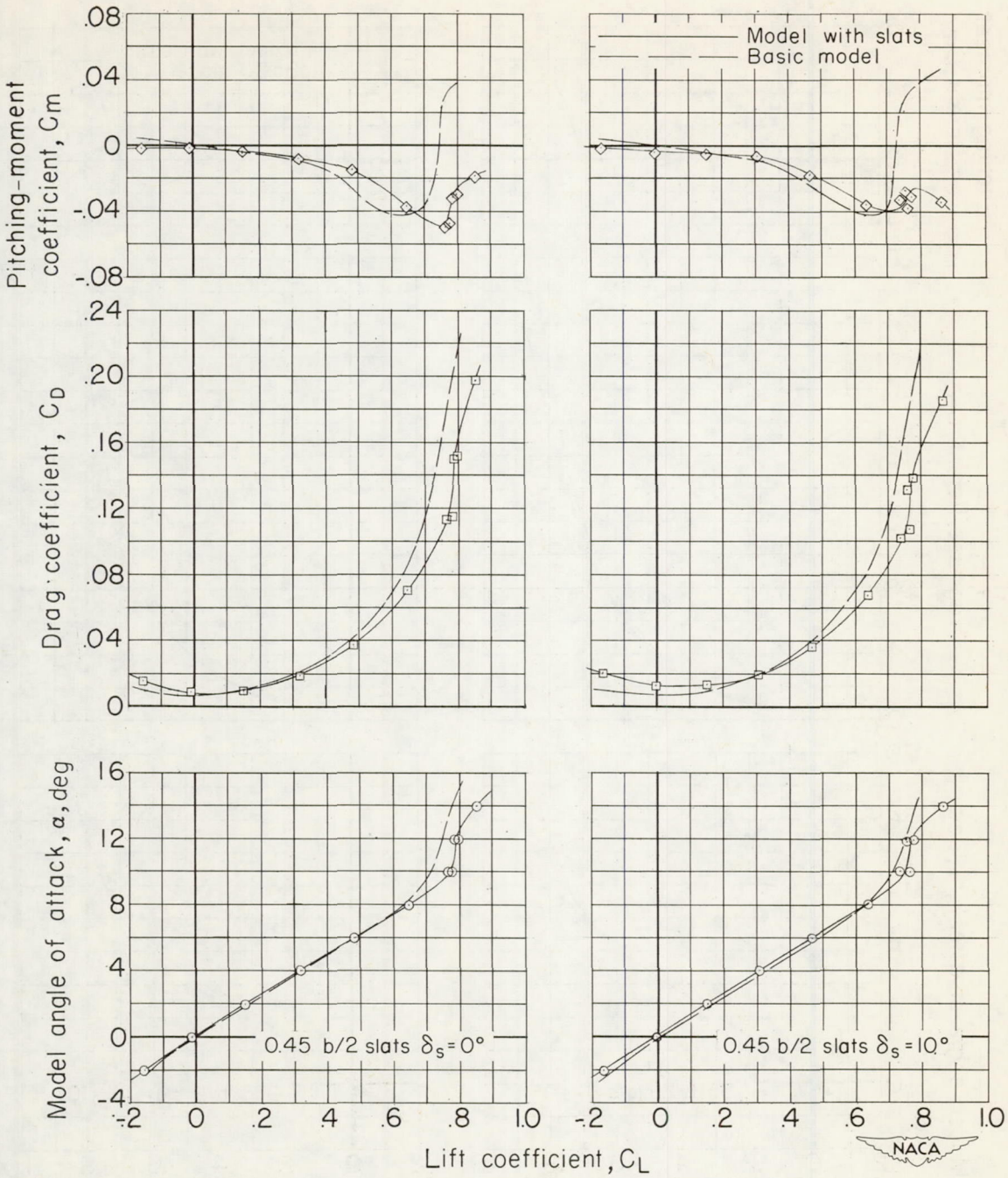

(h) M = 0.90. 0.45b/2 slats, δ_s = 0° and 10°.

Figure 5.- Continued.

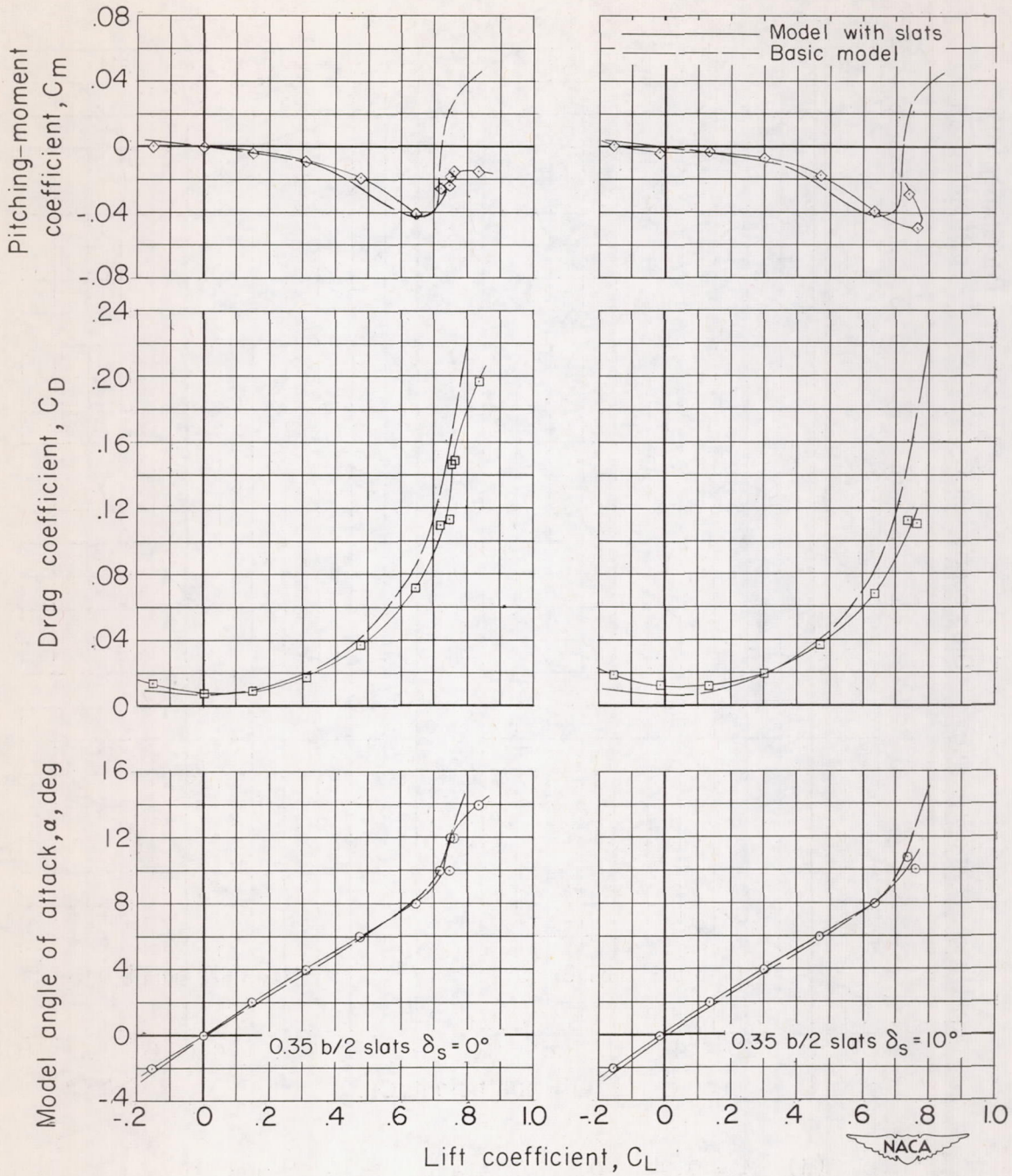

(i) M = 0.90. 0.35b/2 slats, δ_s = 0° and 10°.

Figure 5.- Continued.

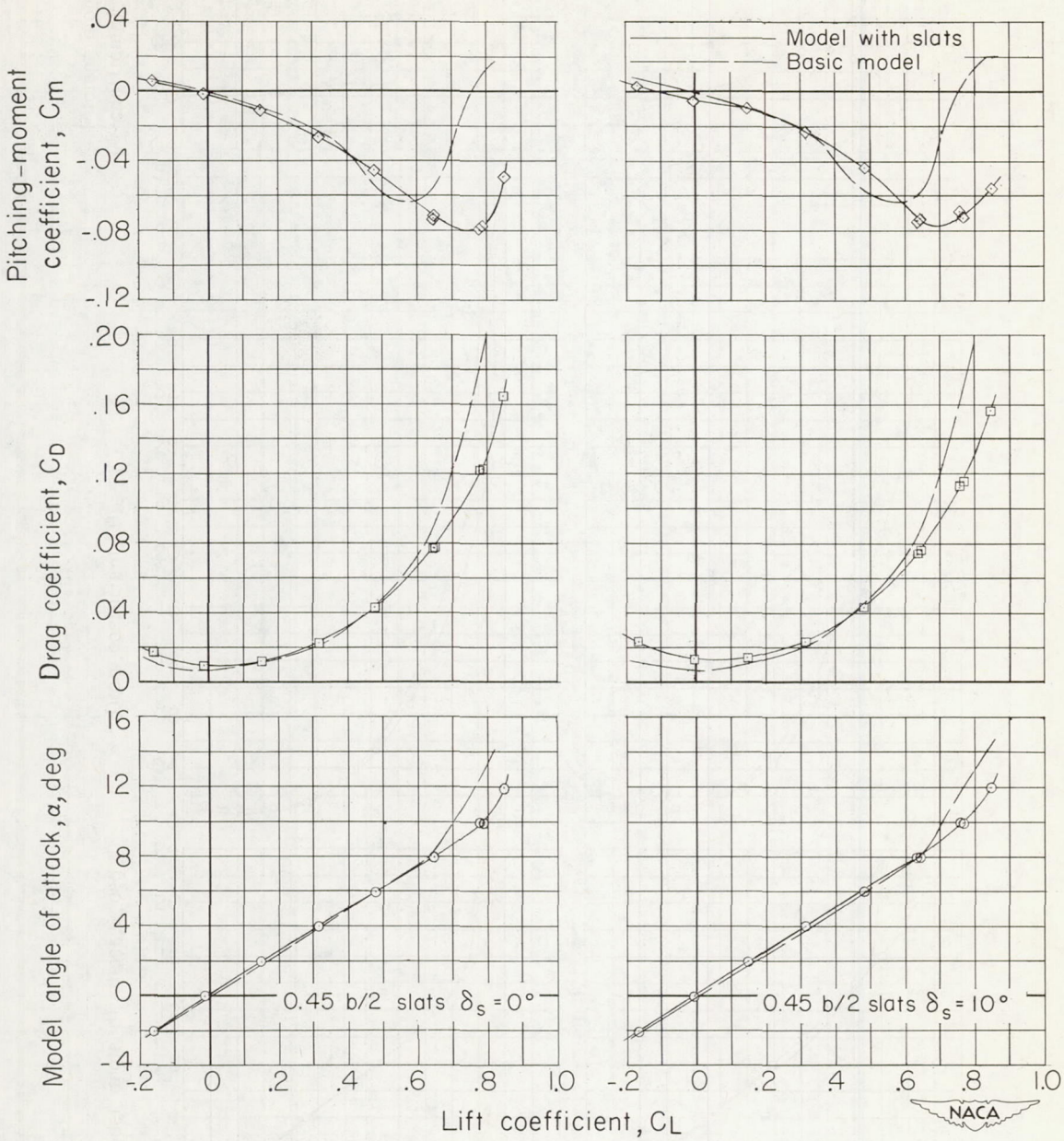

(j) M = 0.94. 0.45b/2 slats, δ_s = 0° and 10°.

Figure 5.- Continued.

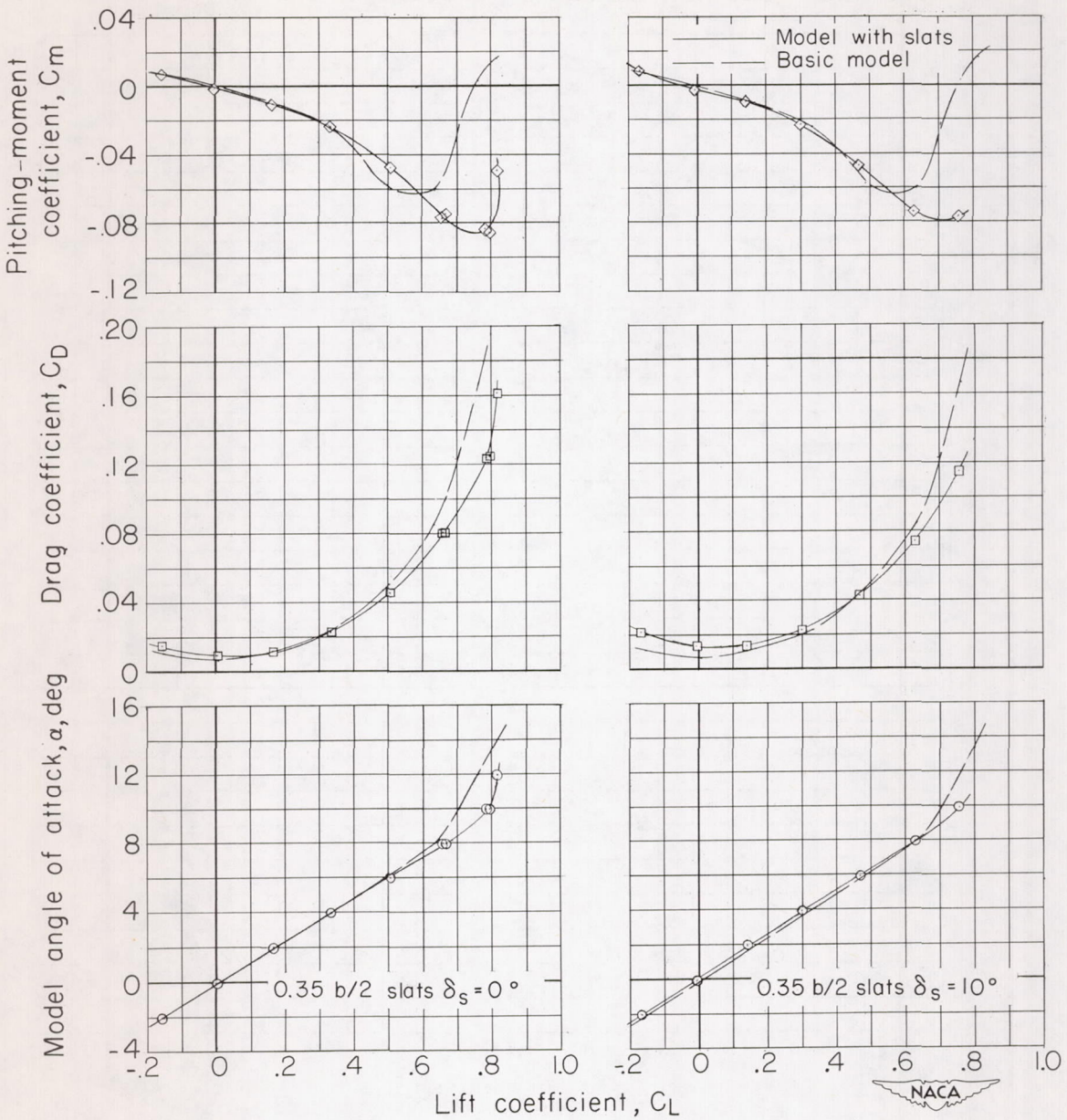

(k) M = 0.94. 0.35b/2 slats, δ_s = 0° and 10°.

Figure 5.- Continued.

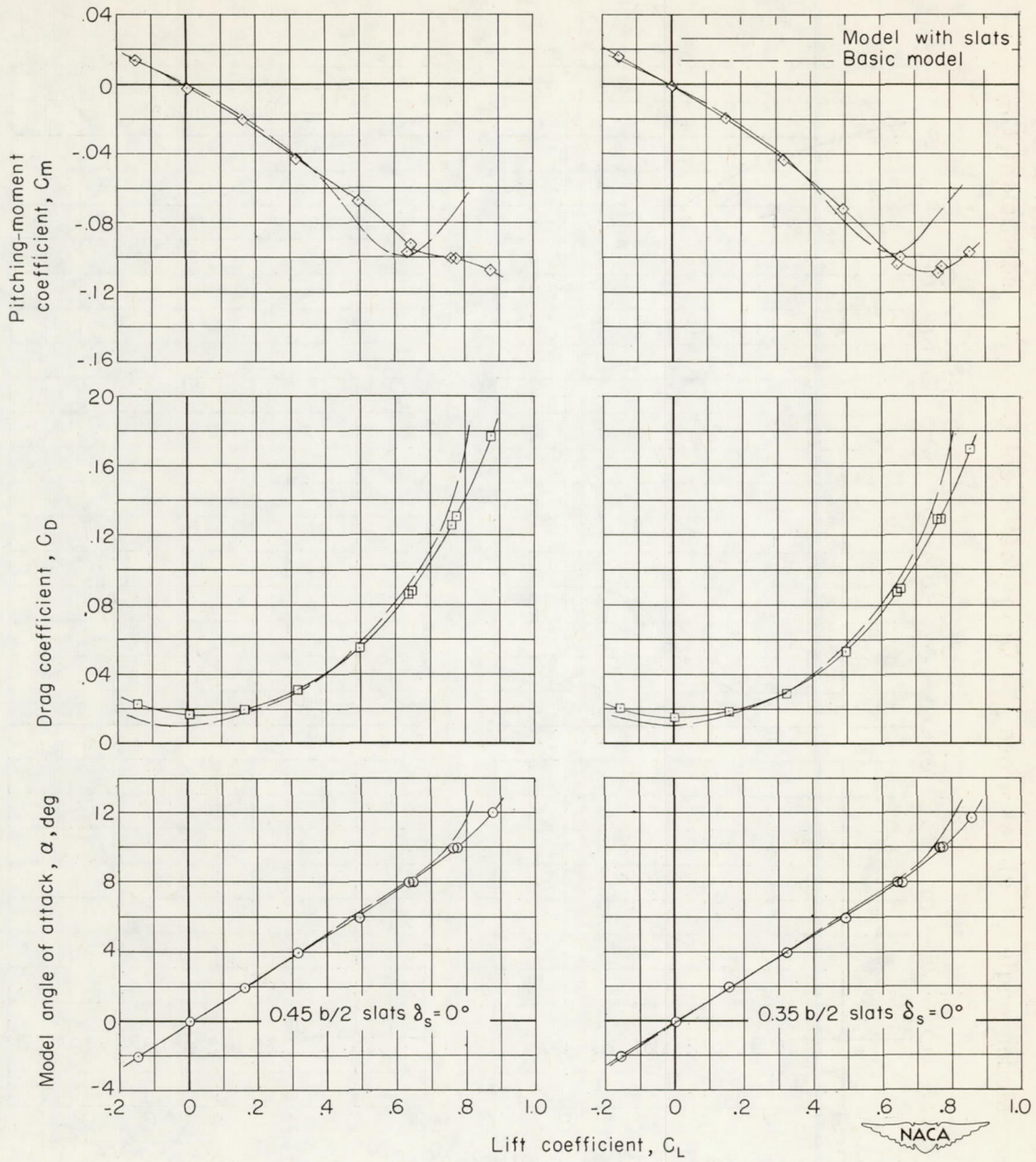

(l) M = 0.98. 0.45b/2 slats, $\delta_s = 0^\circ$; 0.35b/2 slats, $\delta_s = 0^\circ$.

Figure 5.- Continued.

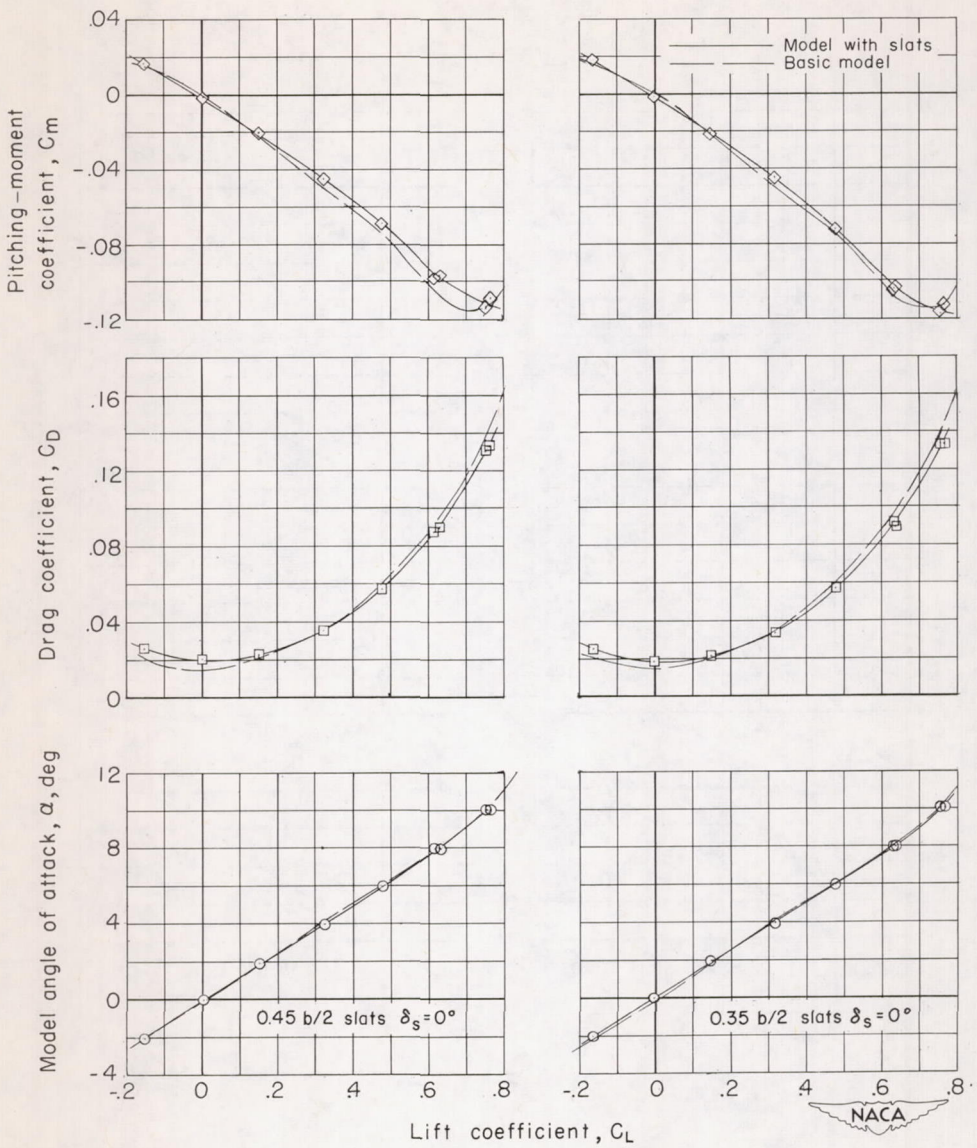

(m) M = 1.00. 0.45b/2 slats, $\delta_s = 0^\circ$; 0.35b/2 slats, $\delta_s = 0^\circ$.

Figure 5.- Continued.

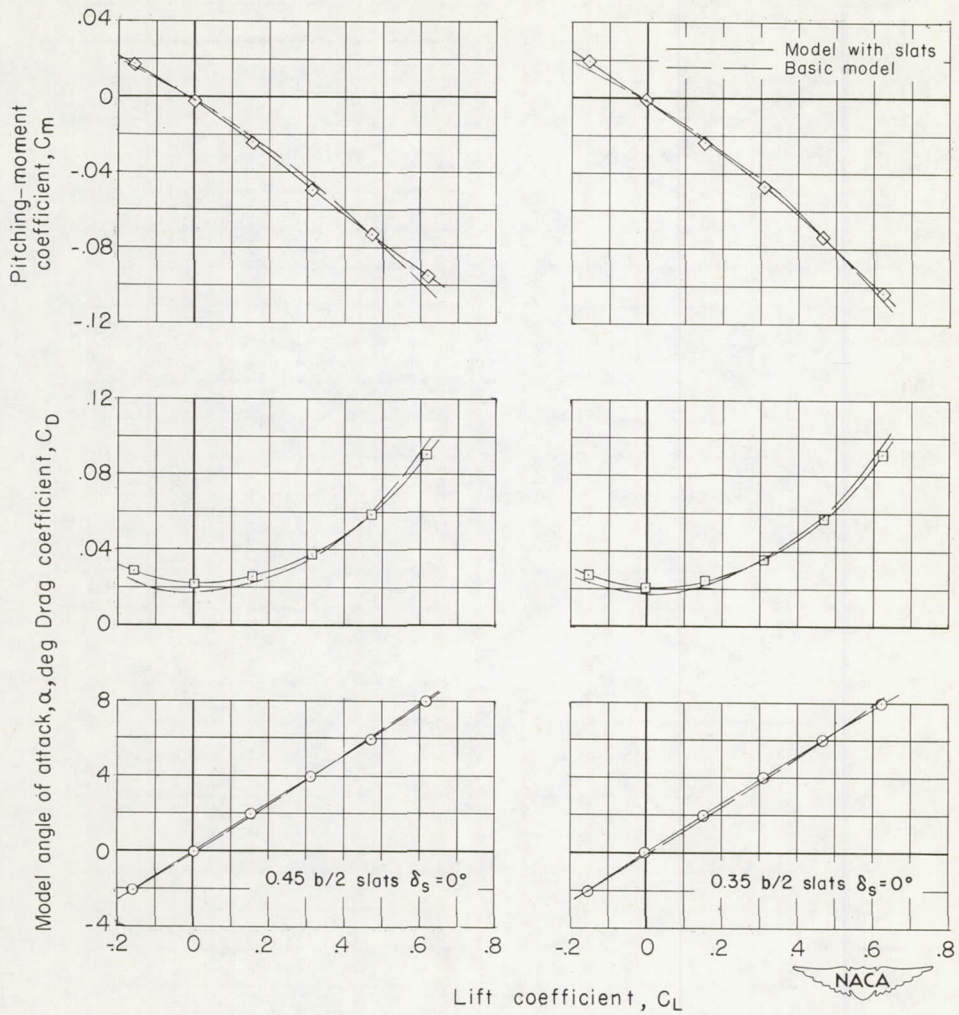

(n) M = 1.03. 0.45b/2 slats, $\delta_s = 0^\circ$; 0.35b/2 slats, $\delta_s = 0^\circ$.

Figure 5.- Concluded.

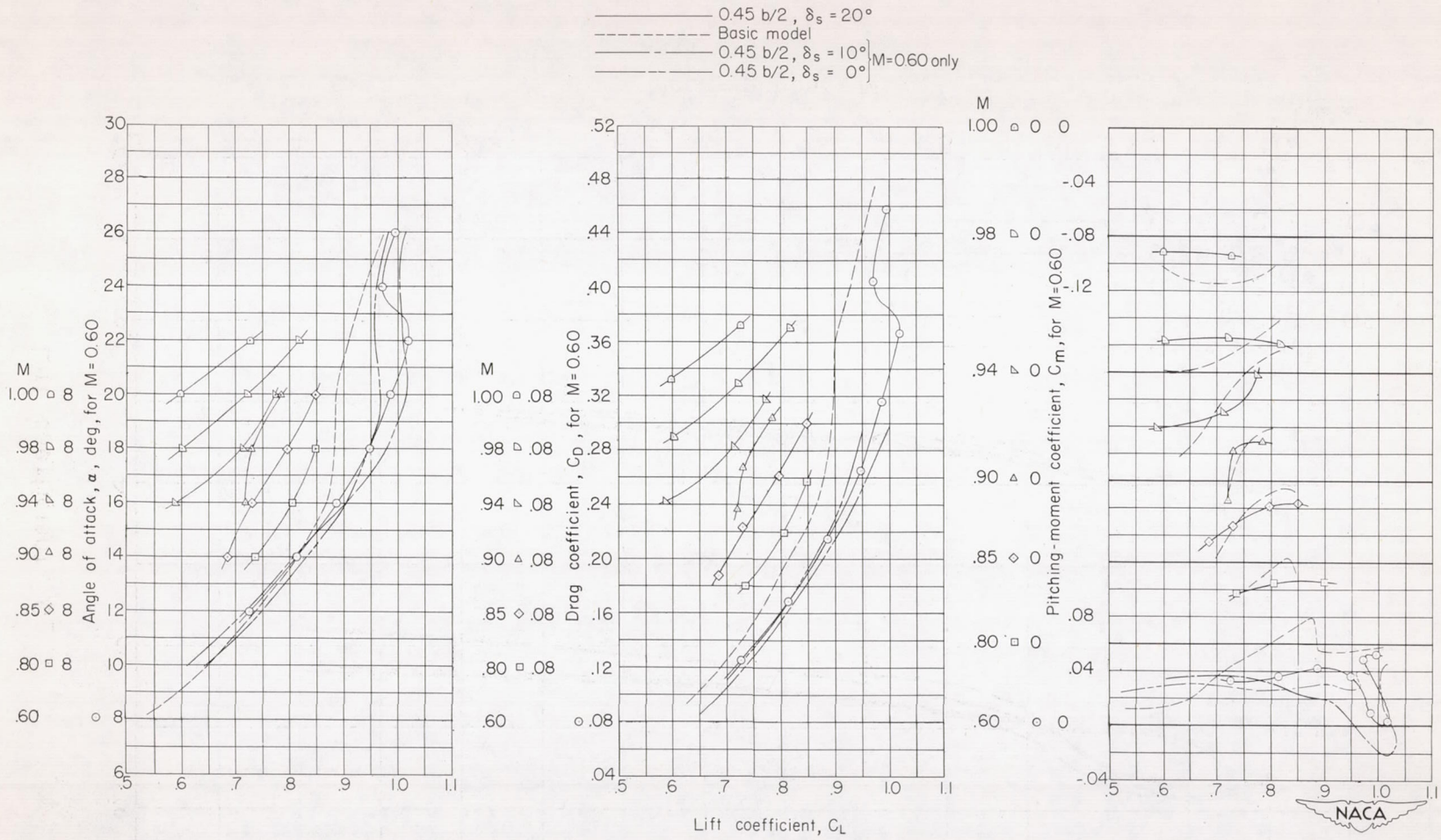

Figure 6.- Aerodynamic characteristics of an 0.45b/2, $\delta_s = 20^\circ$ slat configuration.

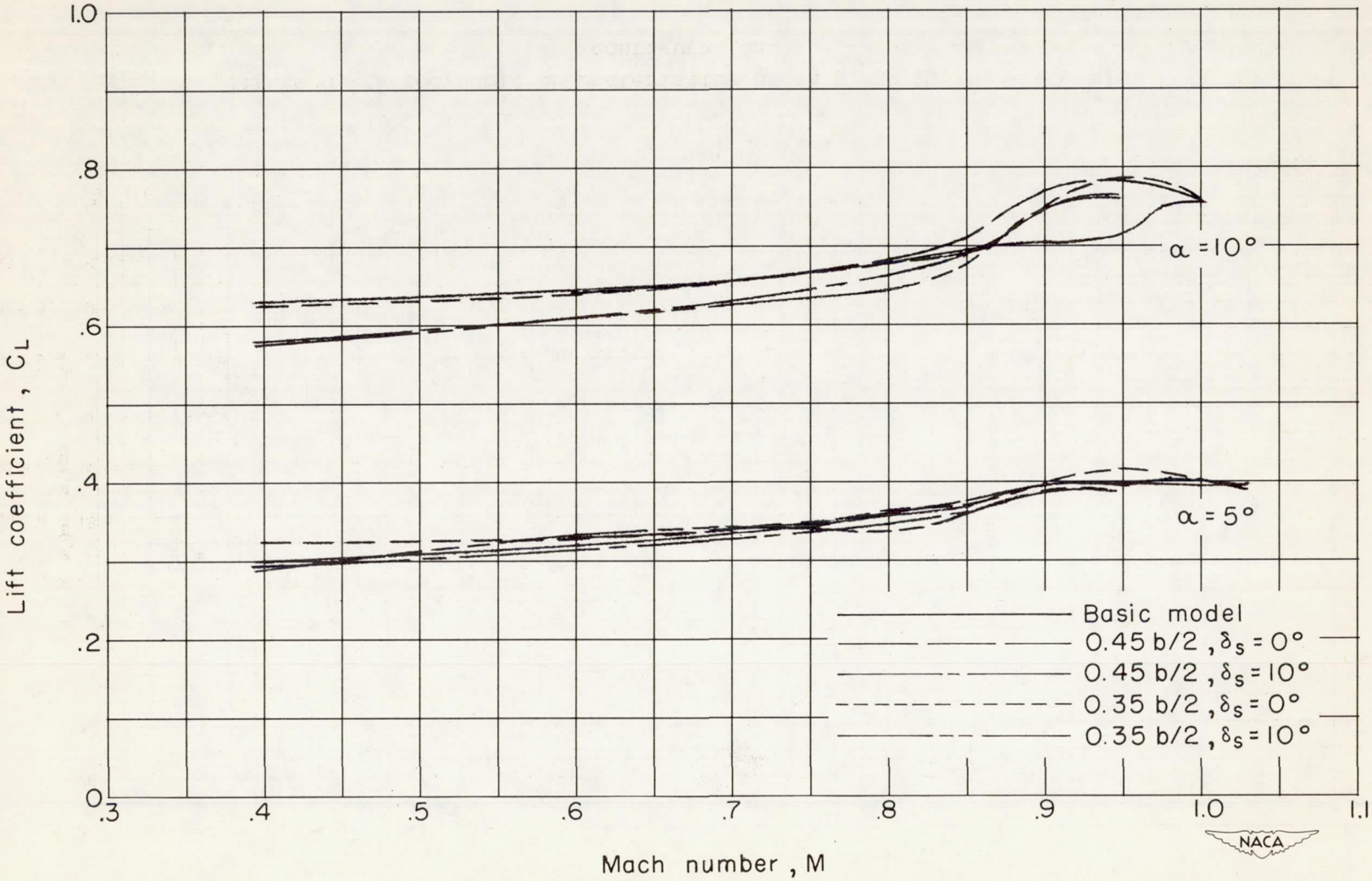

Figure 7.- Variation of lift coefficient with Mach number for basic wing-fuselage combination and configurations with slats.

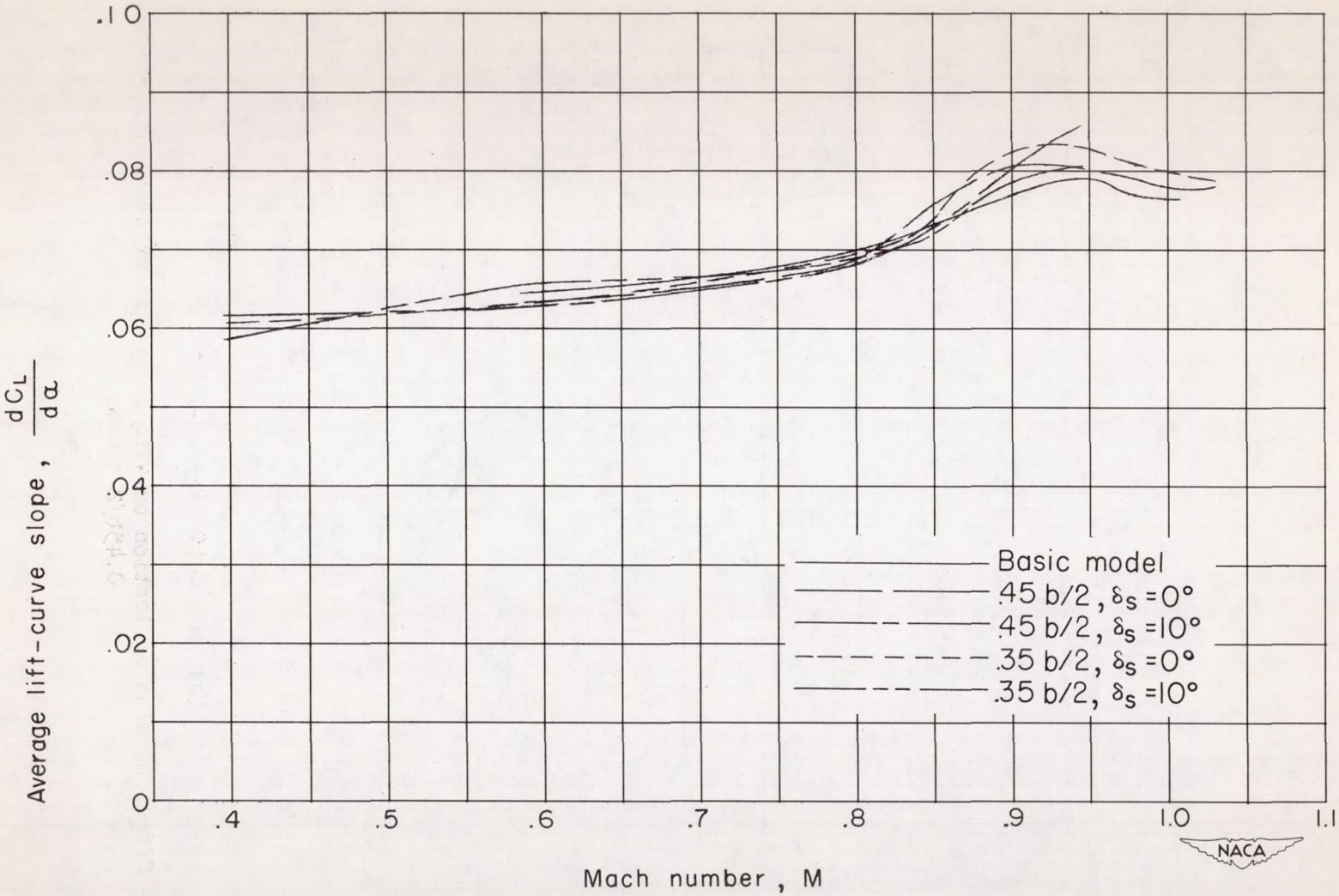

Figure 8.- Variation of average lift-curve slope with Mach number for model with basic wing and configurations with slats. C_L = 0 to 0.4.

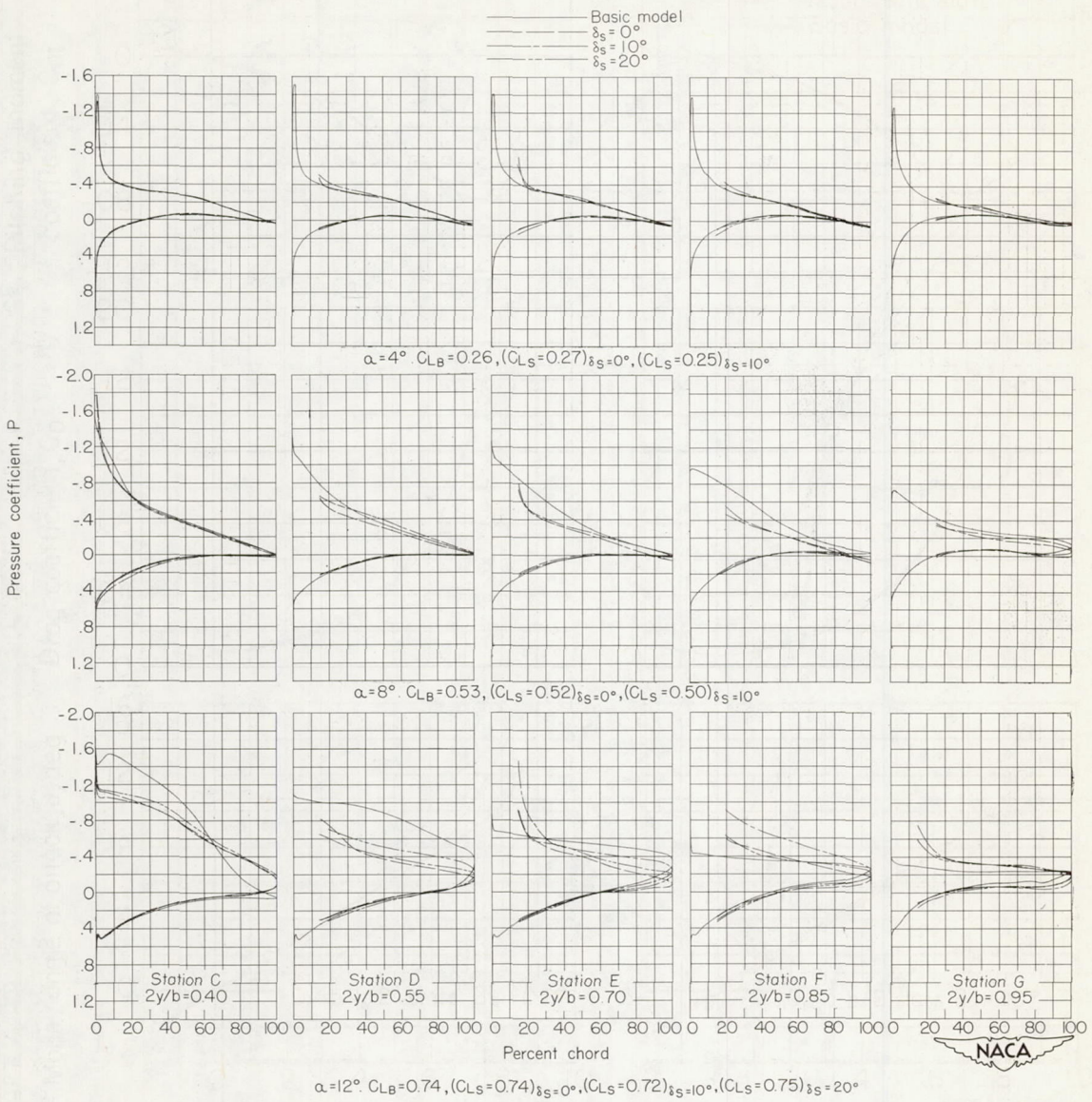

(a) M = 0.60 (P_{cr} = -1.28).

Figure 9.- Effect of slat deflection on wing chordwise pressure distributions. 0.45b/2 slats.

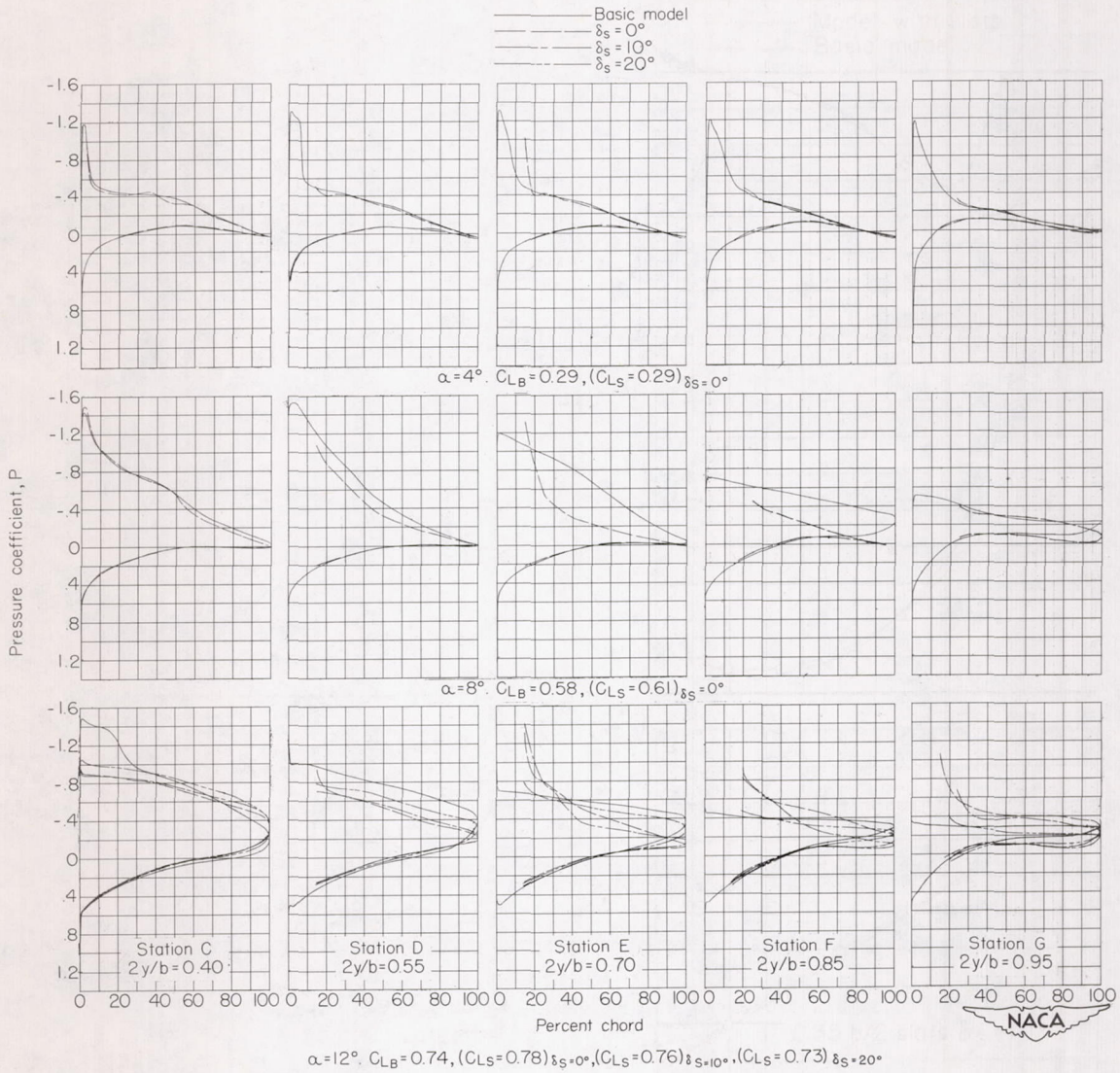

(b) M = 0.85 (P_{cr} = -0.30).

Figure 9.- Continued.

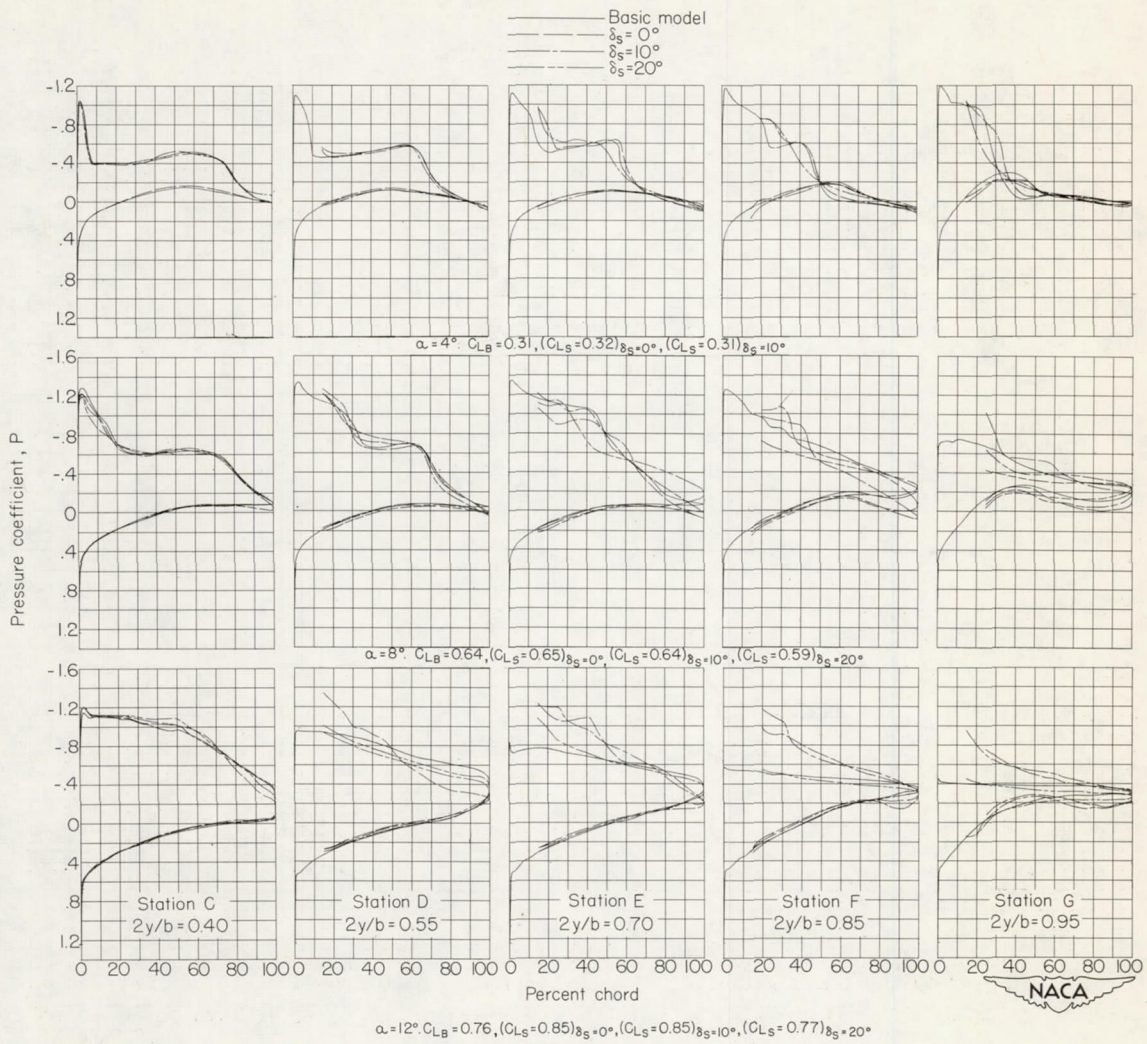

(c) M = 0.94 (P_{cr} = -0.11).

Figure 9.- Continued.

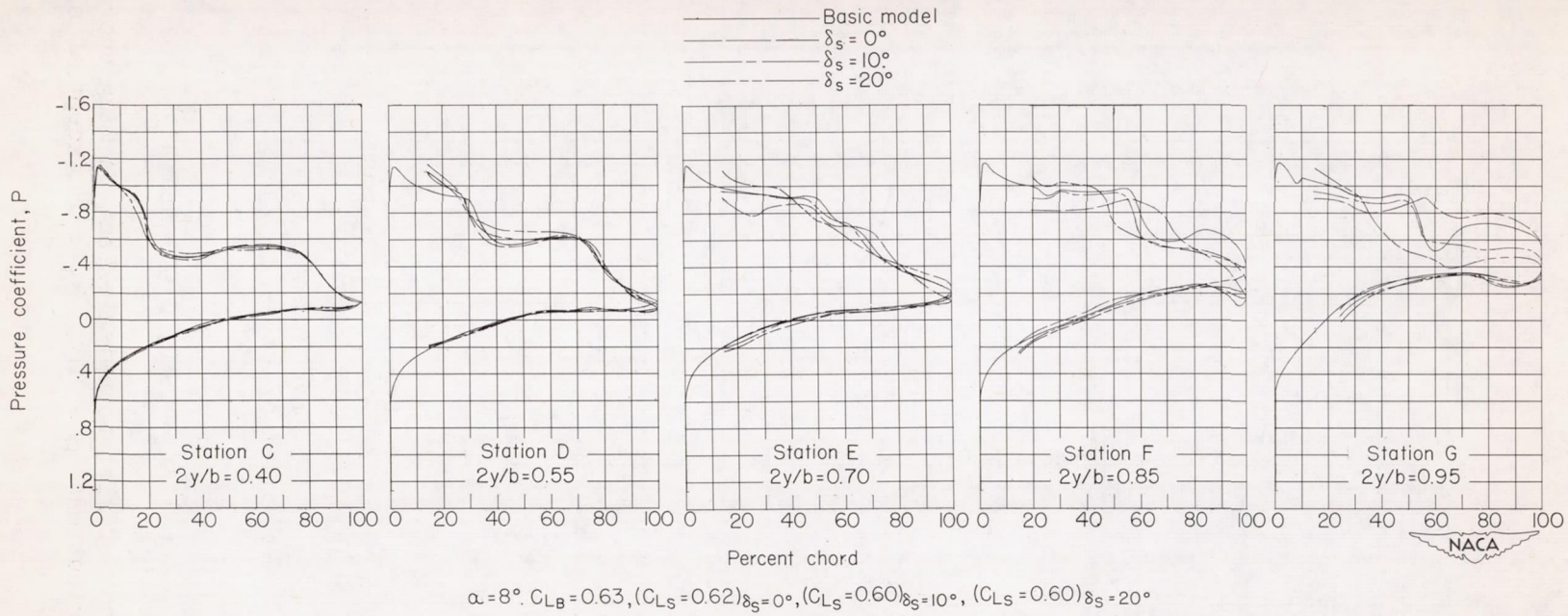

$\alpha = 8°$. $C_{L_B} = 0.63$, $(C_{L_S} = 0.62)_{\delta_S = 0°}$, $(C_{L_S} = 0.60)_{\delta_S = 10°}$, $(C_{L_S} = 0.60)_{\delta_S = 20°}$

(d) M = 1.00.

Figure 9.- Concluded.

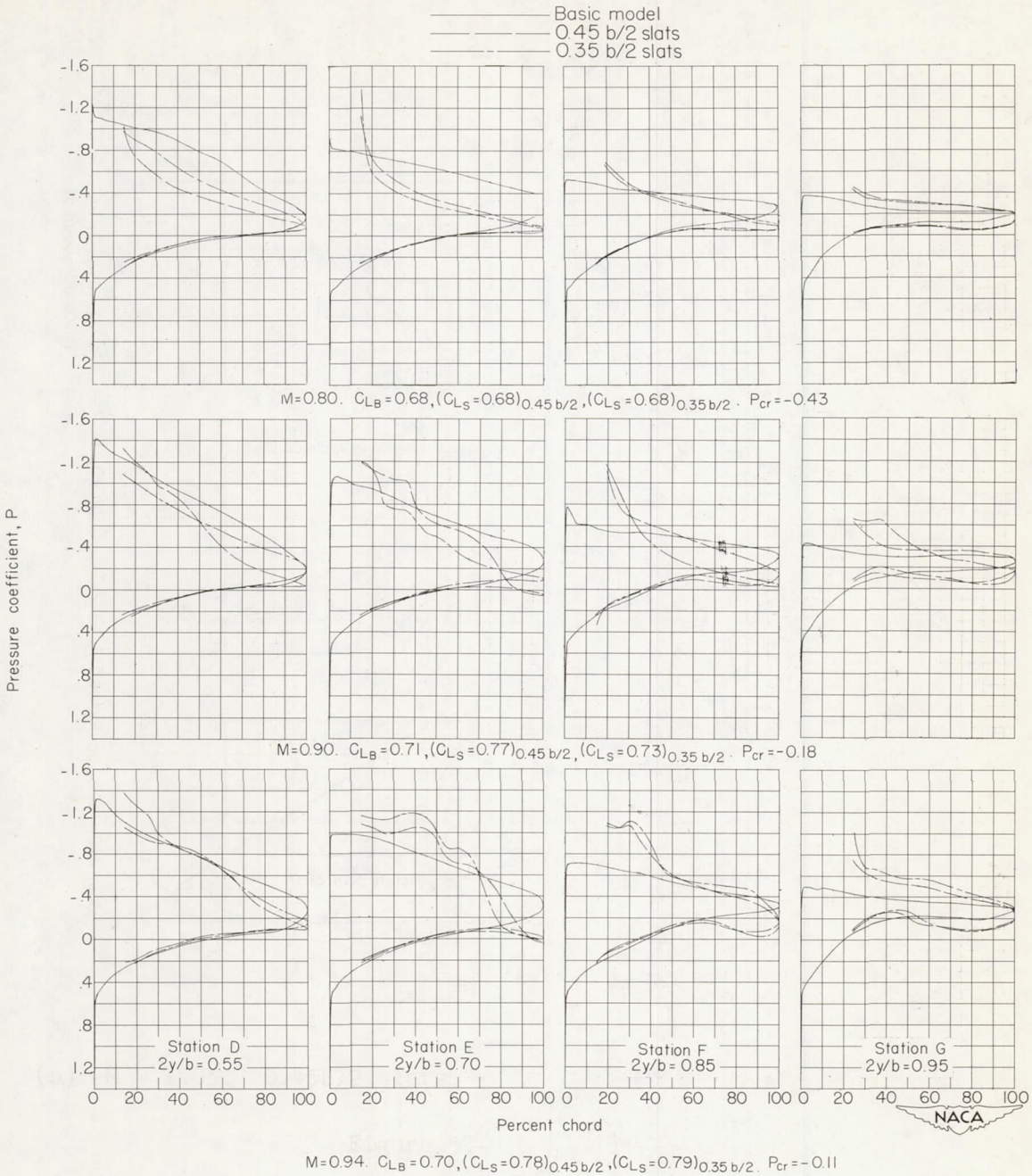

(a) M = 0.80, 0.90, and 0.94.

Figure 10.- Effect of slat spanwise extent on wing chordwise pressure distribution. $\alpha = 10^{\circ}$, $\delta_s = 0^{\circ}$ except as noted.

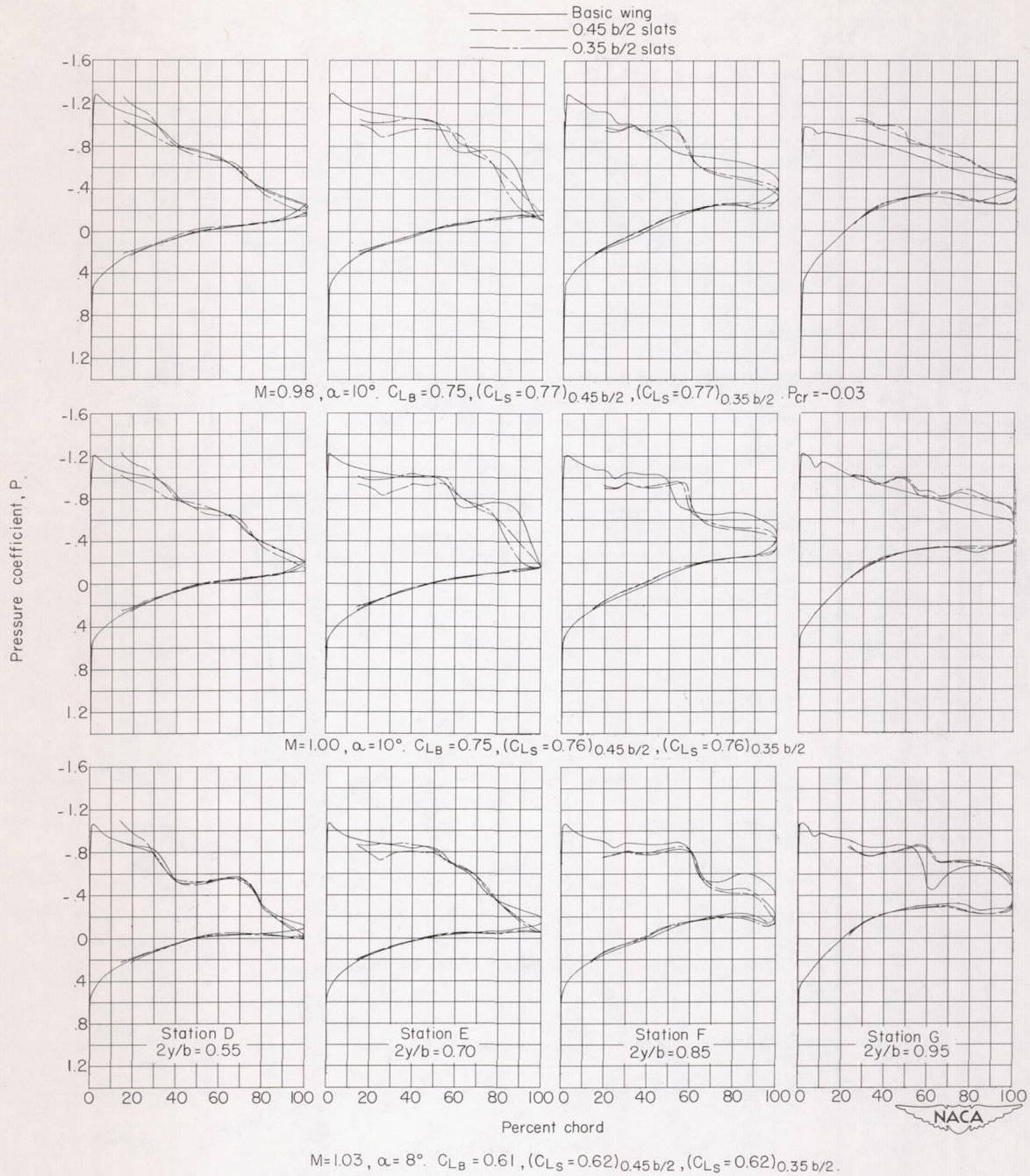

(b) M = 0.98, 1.00, and 1.03.

Figure 10.- Concluded.

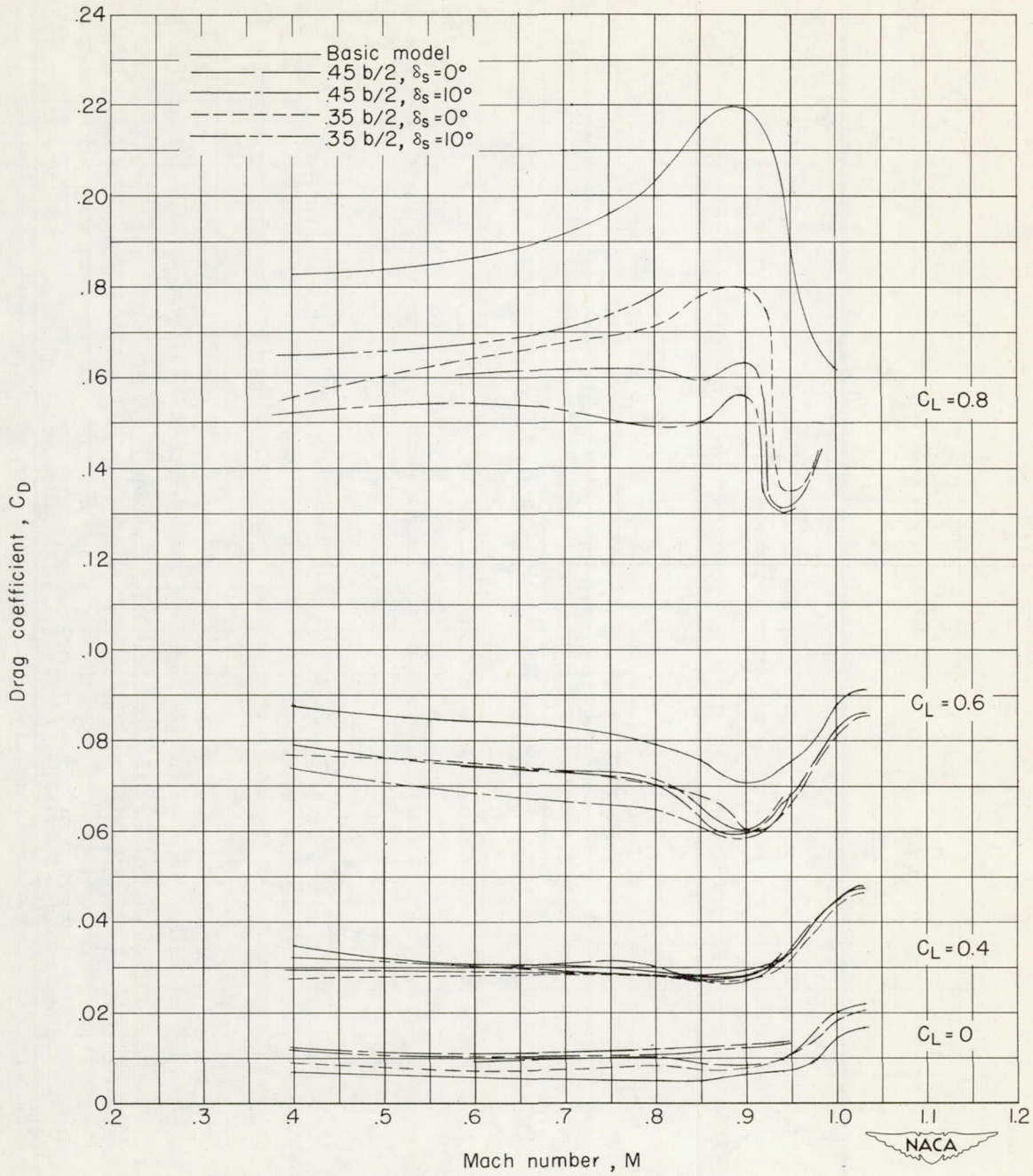

Figure 11.- Variation of drag coefficient with Mach number for basic model and configurations with slats.

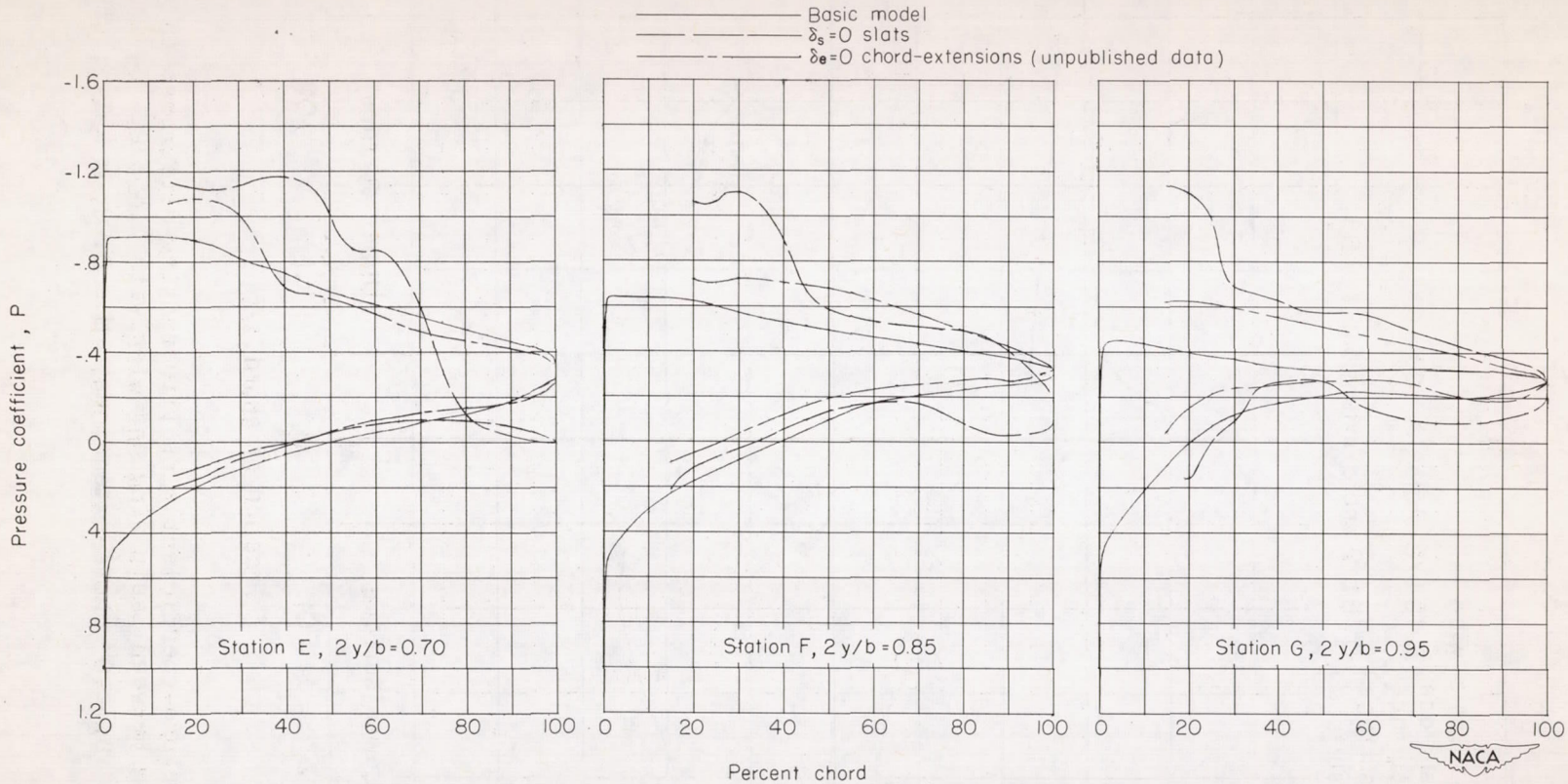

Figure 12.- Typical chordwise pressure distributions obtained with the basic model and with 15-percent-chord and 35-percent-semispan leading-edge devices. $M = 0.94$; $\alpha = 10^{\circ}$. $P_{cr} = -0.11$.

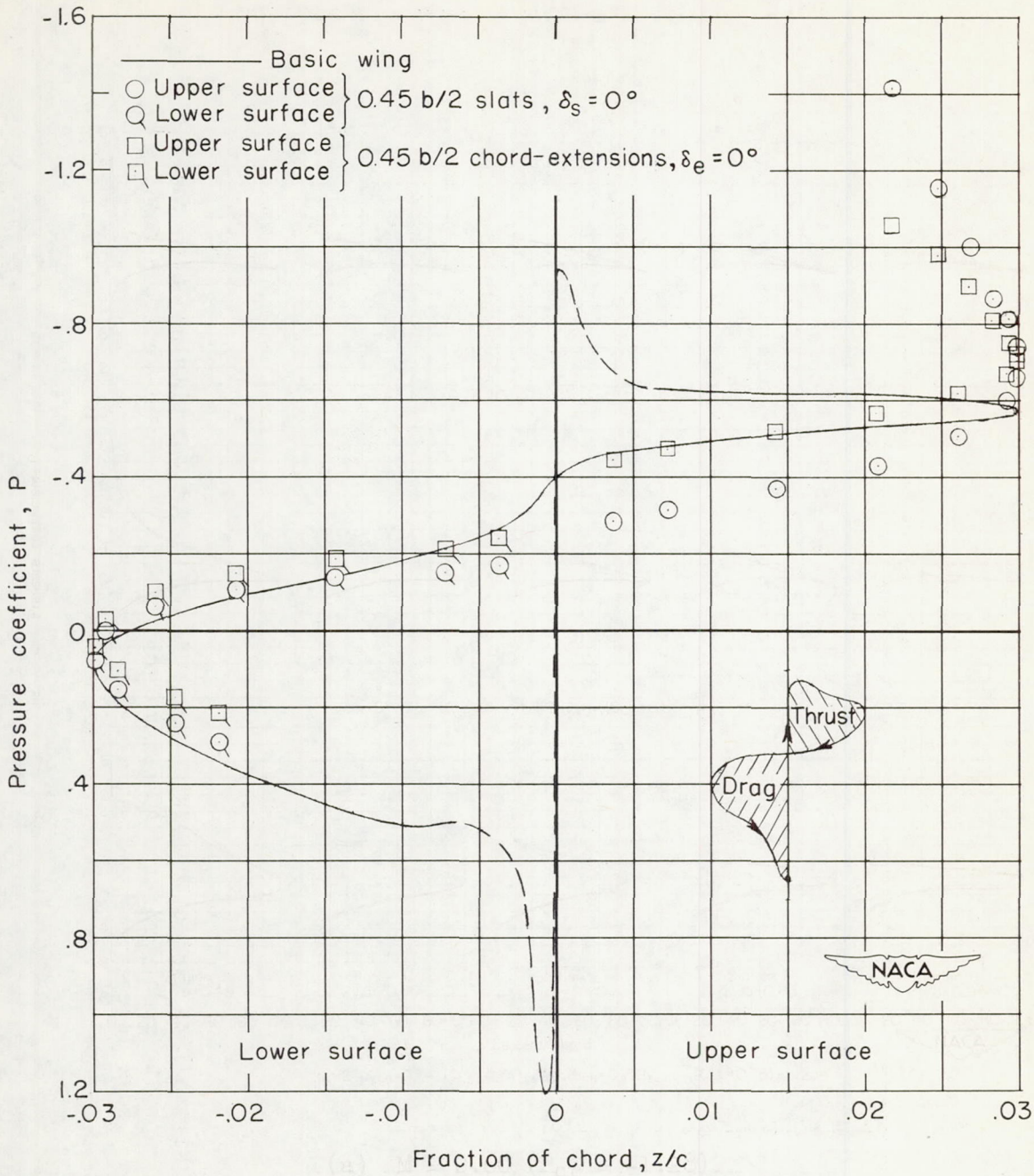

Figure 13.- Pressure-coefficient plot illustrating difference in section pressure drag between basic wing and wing with 0.45b/2, $\delta_s = 0°$ slats and 0.45b/2, $\delta_e = 0°$ chord-extensions. M = 0.90; $\alpha = 14°$; station E, 2y/b = 0.70.

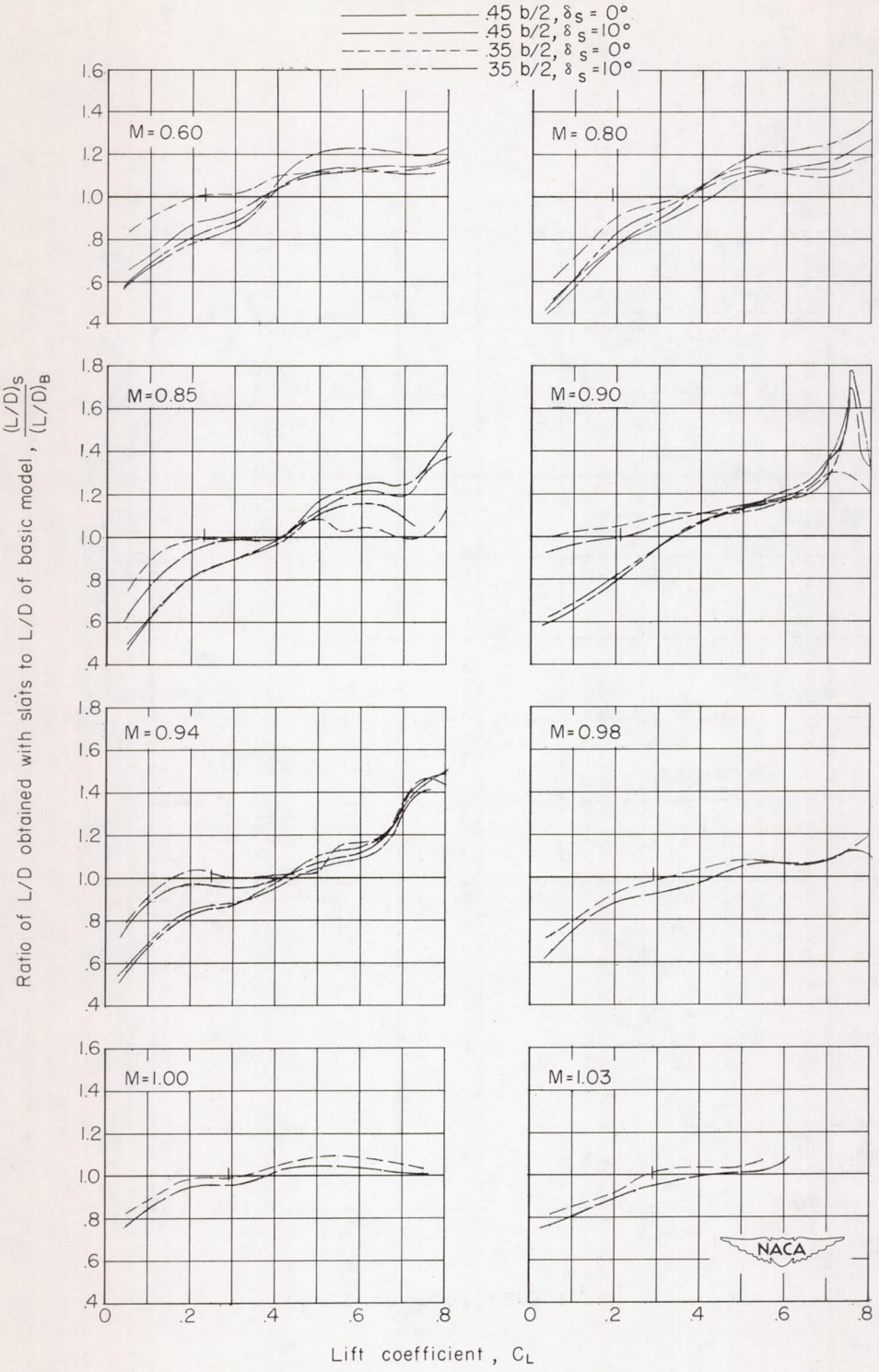

Figure 14.- Ratios of L/D obtained on model with slats to L/D of basic wing-fuselage combination. Ticks indicate C_L for $(L/D)_{max}$ of basic model.

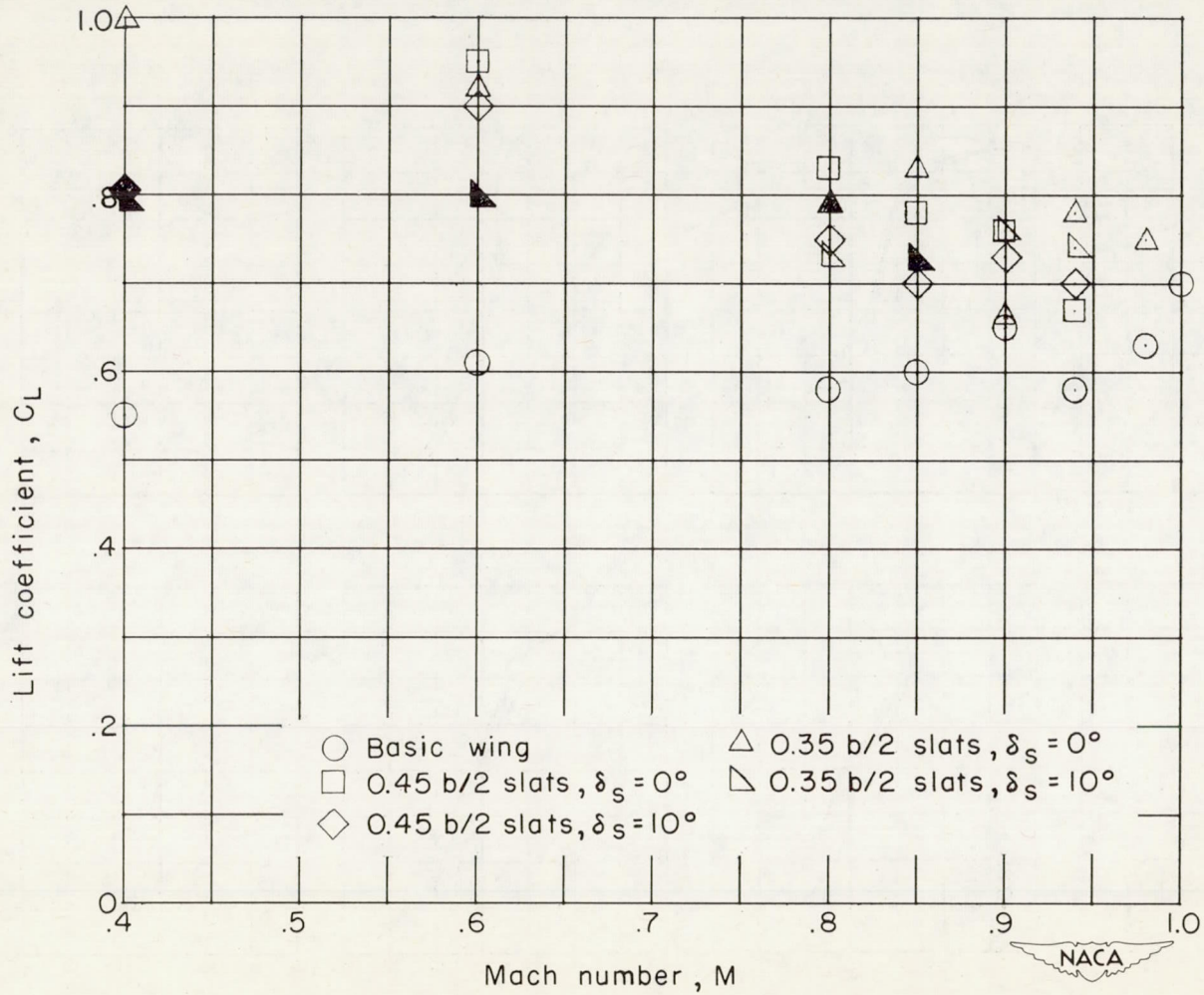

Figure 15.- Lift coefficients at which abrupt stability changes occur for basic wing configuration and configurations with slats. Solid symbol denotes highest lift coefficient obtained in test.

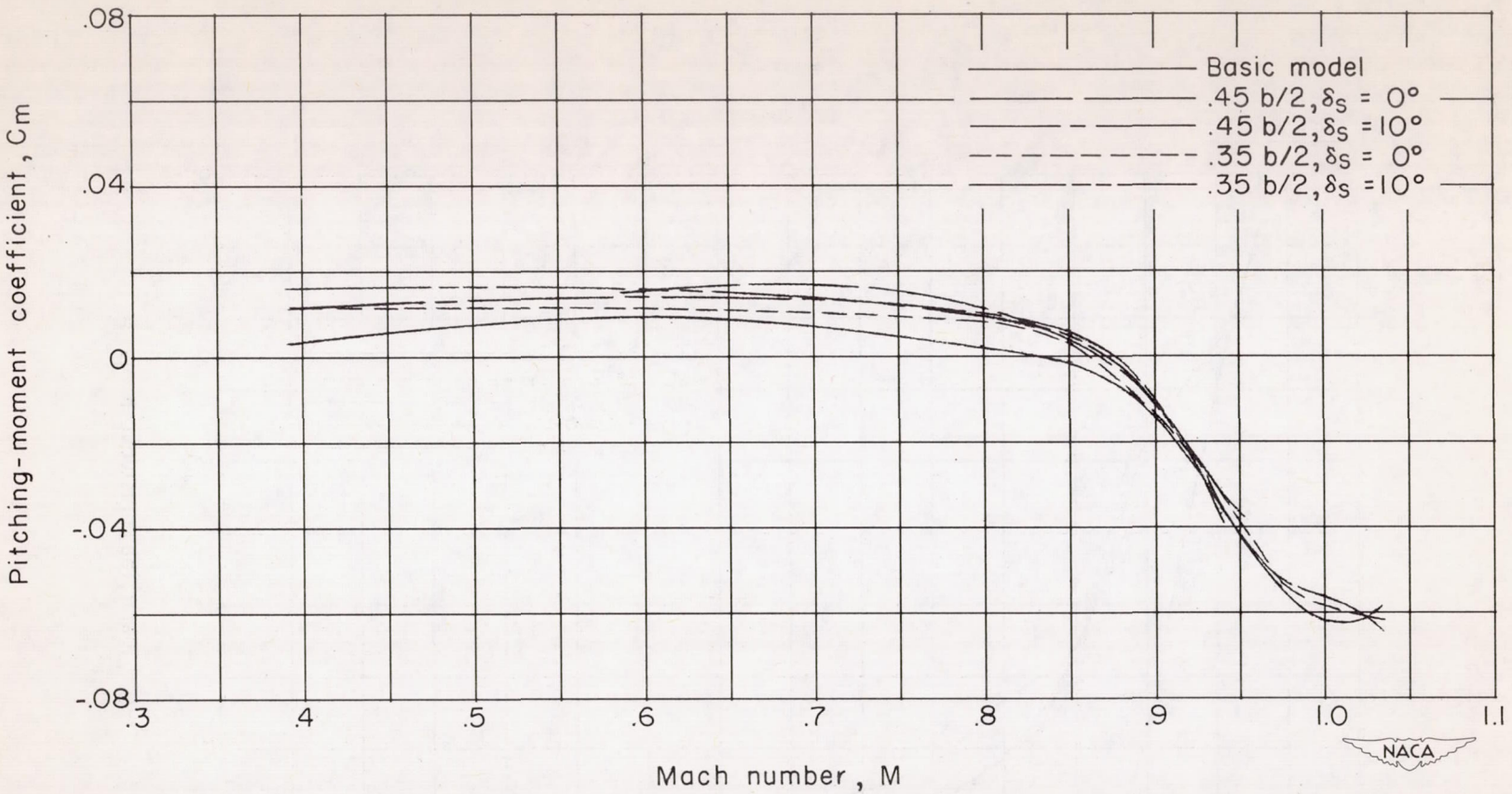

(a) $C_L = 0.4$.

Figure 16.- Variation in pitching-moment coefficient with Mach number for model and wing with slat combinations and basic wing-fuselage model.

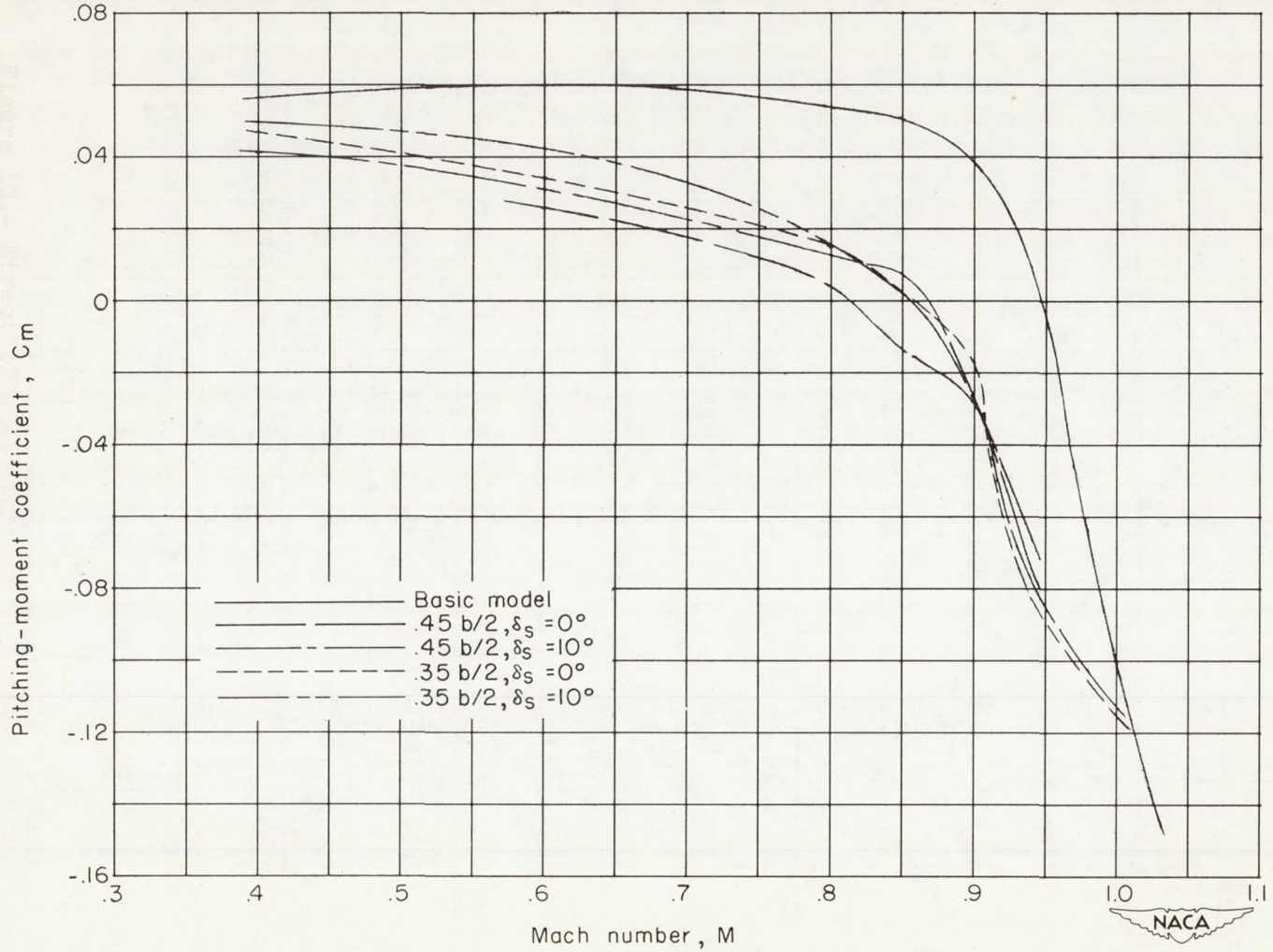

(b) $C_L = 0.8$.

Figure 16.- Concluded.

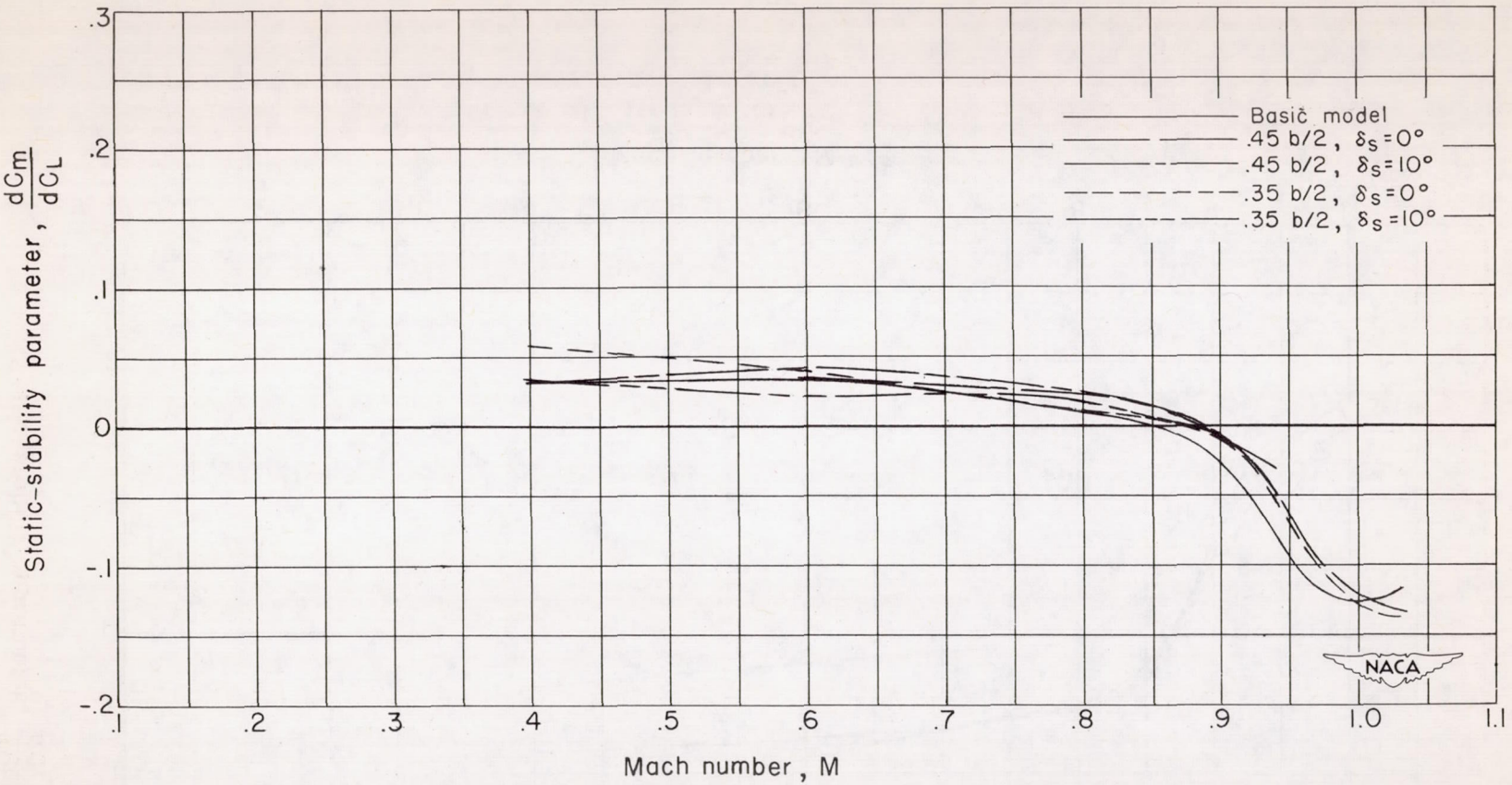

(a) $C_L = 0$.

Figure 17.- Variation of static longitudinal-stability parameter dC_m/dC_L with Mach number for model and wing with slat configurations and for the basic wing-fuselage model.

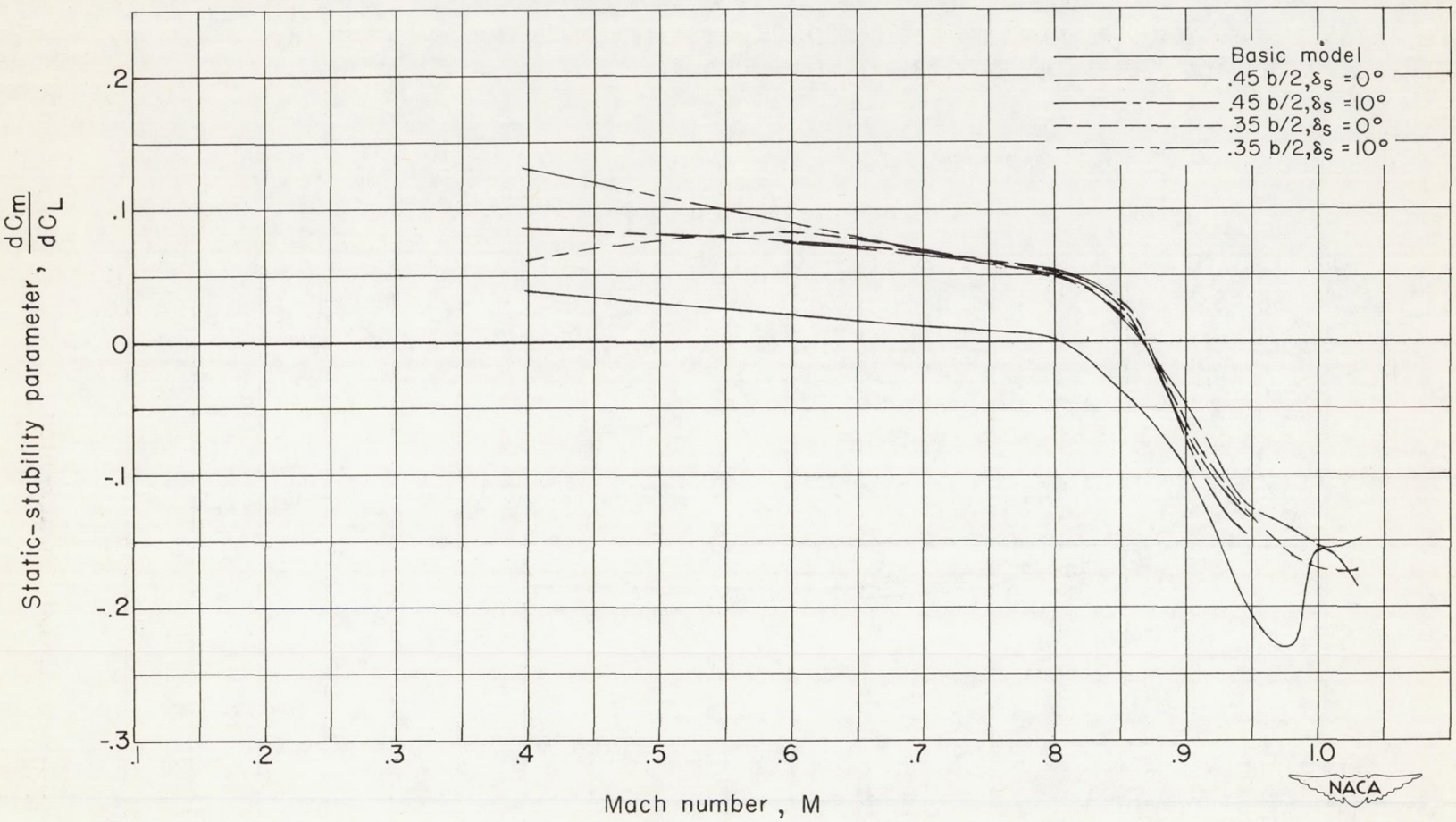

(b) $C_L = 0.4$.

Figure 17.- Concluded.